Z. Angew. Math. Phys. 66 (2015), 2677–2702

0044-2275/15/052677-26
published online March 27, 2015
DOI 10.1007/s00033-015-0521-2

Zeitschrift für angewandte Mathematik und Physik ZAMP

Trapping of surface gravity waves by a vertical flexible porous plate near a wall

R. B. Kaligatla, S. Koley and T. Sahoo

Abstract. The present study deals with the trapping of oblique surface gravity waves by a vertical submerged flexible porous plate located near a rigid wall in water of finite as well as infinite depths. The physical problem is based on the assumption of small amplitude water wave theory and structural response. The flexible plate is assumed to be thin and is modeled based on the Euler–Bernoulli beam equation. Using the Green's function technique to the plate equation and associated boundary conditions, an integral equation is derived which relates the normal velocity on the plate to the difference in velocity potentials across the plate involving the porous-effect parameter and structural rigidity. Further, applying Green's second identity to the free-surface Green's function and the scattered velocity potentials on the two sides of the plate, a system of three more integral equations is derived involving the velocity potentials and their normal derivatives across the plate boundary along with the velocity potential on the rigid wall. The system of integral equations is converted into a set of algebraic equations using appropriate Gauss quadrature formula which in turn solved to obtain various quantities of physical interest. Utilizing Green's identity, explicit expressions for the reflection coefficients are derived in terms of the velocity potentials and their normal derivatives across the plate. Energy balance relations are derived and used to check the accuracy of the computational results. As special cases of the submerged plate, wave trapping by the bottom-standing as well as surface-piercing plates is analyzed. Effects of various wave and structural parameters in trapping of surface waves are studied from the computational results by analyzing the reflection coefficients, wave forces exerted on the plate and the rigid wall, flow velocity, plate deflections and surface elevations. It is observed that surface-piercing plate is more effective for trapping of water waves compared to the bottom-standing and submerged plates. Further, irrespective of plate configurations, full reflection occurs for the same values of the distance between the plate and the rigid wall. Similar phenomenon is observed in case of angle of incidence. Irrespective of plate configurations, in the very long wave regime, full reflection occurs in case of partial plate of any length due to the occurrence of the wave diffraction through the gap region while zero reflection occurs in case of fully extended plate.

Mathematics Subject Classification. 76B15.

Keywords. Wave trapping · Flexible porous plate · Green's function · Integral equation · Reflection coefficient.

1. Introduction

One of the greatest menaces to the mankind is the rise of seawater level due to global warming. The significant increase in real estate along the coast, due to the rise in world population, is likely to exert even greater pressure on the coastal cities and island countries for designing coastal structures for shore protection keeping in mind the rise in sea level. Further, the significant rise in global trade and transport is putting additional pressure on the existing ports and harbors. With an increase in global trading, there is a substantial increase in harbor traffic on account of movement of large number of ships results in the deterioration of wave conditions in various ports and harbors around the world. Field measurements reveal that most of the wave energy incident upon harbor walls is reflected back and worsen the wave climate during the peak hours within harbors. Over the years, vertical rigid walls have been constructed for protection of marine facilities in coastal zones. However, many of these vertical rigid walls have collapsed due to high wave loads. To reduce wave loads on these existing walls, various permeable structures such as perforated caisson-type sea walls, piled barriers and slotted vertical walls have been suggested (see [1]). Further, to minimize wave loads on coastal structures like sea walls, it is found that a complete or

partial porous structure can be kept at a suitable distance from the vertical wall and thus developing a wave trapping system. Also, for creating a tranquility zone, flexible and porous partial barriers are proposed as alternatives. In the design of an effective wave trapping system for protecting marine facilities, complete/partial flexible porous structures are proposed as temporary barriers in the vicinity of marine structures. Moreover, flexible porous wave barriers which consist of vertical porous membrane acting under tension are proposed to increase the effectiveness of wetlands habitat restoration projects (see [2]).

In the absence of end wall in a channel, studies on water wave scattering by partial rigid barriers started since Dean [3] who studied the surface gravity wave reflection by a thin submerged barrier in infinite water depth. Ursell [4] studied the wave scattering by surface-piercing barrier using Havelock's expansion of velocity potential in infinite water depth. Since then, various mathematical techniques were developed to tackle mixed boundary value problems involving different barrier configurations. Mandal and Chakrabarti [5] extensively reviewed the numerous methods to study wave scattering by partial rigid barriers. Further, in the book of Linton and McIver [6], a wide range of mathematical techniques are described to deal with wave-structure interaction problems in broad fields of research including water waves. In these studies, the structure was assumed to be rigid in nature. Sahoo [7] discussed several mathematical techniques used in the literature for analyzing wave interaction with flexible and porous barriers of various configurations. On the other hand, Meylan [8] studied water wave scattering by a surface-piercing vertical flexible sheet by using Fredholm- type integral equations and Green's function technique. Following Meylan's approach, Chakraborty and Mandal [9,10] studied water wave scattering by a submerged flexible plate in water of finite and infinite water depths, respectively. Recently, Koley et al. [11] studied oblique wave scattering by a submerged flexible porous plate in both the cases of finite and infinite water depths. In the solution procedure, using free-surface Green's function and Green's identity, the boundary value problem is converted into a system of three integral equations which are handled for solution numerically. Also, energy identities for wave scattering by flexible porous barriers are derived and used to check the accuracy of the numerical results obtained in several cases.

In the literature, studies on the existence of trapped waves started since Stokes [12] demonstrated the existence of edge waves along a sloping beach. Ursell [13] demonstrated the existence of trapped modes traveling along the top of a fully submerged infinite circular cylinder, having sufficiently small radius and parallel to free surface in a channel of infinite water depth. Subsequently, Jones [14] generalized Ursell's result to prove the existence of trapped modes in the presence of cylinders of arbitrary cross section which is symmetric about vertical axis. Greenspan [15] found trapped and interfacial waves in a constantly stratified fluid over a sloping beach. Later on, several investigations were carried out in different situations on the existence of trapped waves. Leblond and Mysak [16] highlighted the importance of edge waves/trapped modes in the dynamics and sedimentology of the nearshore zones. Linton and Evans [17] analyzed the existence of trapped modes above a horizontal submerged flat plate in water of finite depth. Linton and McIver [18] found the occurrence of zero reflection for any given incident wavenumber when a circular cylinder is submerged horizontally in the lower layer of two-layer fluid of infinite depth. An extensive literature survey on the mathematical theory of trapped waves for different geometrical situations can be found in Kuznetsov et al. [19]. In all these studies, the emphasis was on showing the existence of trapped waves. These trapped waves correspond to the time-harmonic free oscillation of water surface confined to a finite region as defined by Sahoo et al. [20].

In the context of wave interaction with porous structures, Chwang and Dong [21] developed a wave trapping system by introducing a vertical porous plate near the end of a semi-infinite long channel of uniform depth. This study was further generalized by Wang and Ren [22] to analyze wave trapping by a flexible porous barrier located at a finite distance from a rigid wall in a channel of finite depth. Sahoo et al. [20] analyzed trapping as well as generation of surface waves by partial permeable barriers of different configurations located near the end of a semi-infinitely long channel of finite depth. Yip et al. [23] extended the study on wave trapping to include flexibility in the porous barriers. Behera et al. [24] investigated oblique wave trapping system in a two-layer fluid of finite depth. In the aforementioned problems, the

barrier is assumed to be of negligible width. On the other hand, oblique wave trapping by porous structures of finite width was studied by Koley et al. [25]. Behera and Sahoo [26] analyzed oblique wave scattering and trapping by porous structures of finite width having various configurations in water of finite depth in two-layer fluid. Also, they considered a porous structure with perforated front and rigid back walls as special cases. In all these class of problems, the objective was on finding the optimum distance between the porous structure and the end wall for which wave reflection attends minimum value. The case of zero reflection is referred as full-wave trapping, while the case for which nonzero minimum in wave reflection occurs is referred as partial wave trapping. In most of these studies on wave trapping mentioned above, the physical problems are handled using classical methods such as eigenfunction expansion method, least-square approximation method and boundary element method. In the boundary element method, free-space Green's function is used and one has to deal with a large matrix system for the accuracy of the solution. Further, all these problems were handled in water of finite depth. To the authors knowledge, no study on wave trapping by porous and flexible structures is available in the literature in the case of infinite water depth.

In the present paper, oblique wave trapping by a vertical submerged flexible porous plate located near a vertical rigid wall is analyzed. As special cases of the submerged flexible plate problem, oblique wave trapping by surface-piercing and bottom-standing partial flexible porous plates are analyzed. Using the free-surface Green's function and Green's identity, the mixed boundary value problem is converted into a system of four integral equations. The integrals associated with the integral equations are evaluated using Gauss–Legendre quadrature formulae in case of finite water depth and Gauss–Laguerre quadrature formulae in case of infinite water depth. With suitable application of Green's identity and far-field condition, expression for reflection coefficient is obtained in terms of the velocity potentials and their normal derivatives. Furthermore, using Green's identity, energy relations are derived in both the cases of finite and infinite water depths and are used to check the accuracy of various computational results. To understand the effectiveness of the flexible porous plates in trapping oblique waves, various numerical results on reflection coefficients, wave loads on the plate and the rigid wall, plate deflection, free- surface elevation and flow field are presented in both the cases of water of finite and infinite depths. A comparative study on wave trapping by flexible porous plates located near a wall is demonstrated between finite and infinite water depths by analyzing the reflection coefficients and forces acting on the flexible porous plate.

2. Formulation of boundary value problem

The physical problem associated with oblique surface wave trapping by flexible submerged porous plate is studied in the three-dimensional Cartesian coordinate system in both the cases of water of finite and infinite depths under the assumption of classical small amplitude water wave theory and structural response. The fluid domain is assumed to be infinitely extended in the x–z horizontal directions as $-\infty < x, z < \infty$ with y-axis being taken vertically downward and the horizontal plane $y = 0$ being the undisturbed free surface. A flexible porous plate is assumed to be kept at $x = 0$ at a finite distance L from a rigid wall in a semi-infinite long channel as in Fig. 1. As special cases of the submerged plate, wave trapping by surface-piercing and bottom-standing flexible porous plates is studied. For notational convenience, L_{p} refers to the plate region and L_{g} refers to the gap region above and/or below the plate. Further, in the case of finite water depth, $L_{\mathrm{p}} = (0, b)$ for surface-piercing plate, (a, b) for submerged plate and (a, h) for bottom-standing plate while, the corresponding gap regions are given by $L_{\mathrm{g}} = (b, h)$, $(0, a) \cup (b, h)$ and $(0, a)$. On the other hand, in the case of infinite water depth, $L_{\mathrm{g}} = (b, \infty)$ for surface-piercing plate and $L_{\mathrm{g}} = (0, a) \cup (b, \infty)$ for submerged plate. In the present study, bottom-standing plate in infinite water depth is not considered since such a structure in practice is physically irrelevant in nature. The fluid is assumed to be incompressible, inviscid with motion being irrotational and simple harmonic in time with

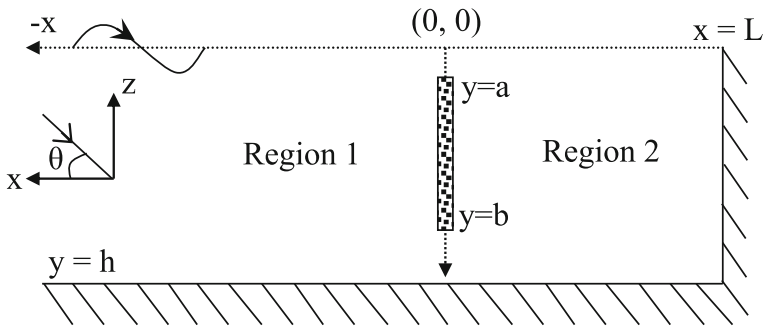

FIG. 1. Schematic diagram for oblique wave trapping by a flexible porous plate near a wall

angular frequency ω. Further, it is assumed that the surface waves are incident upon the plates making an angle θ with x-axis. Thus, there exist velocity potentials of the form $\Phi_j(x,y,z,t) = Re\{\phi_j(x,y)e^{i(k_z z-\omega t)}\}$ with k_z being the z-component of the plane progressive wave incident upon the plate and subscripts $j = 1, 2$ referring to the fluid domains 1 and 2 shown in Fig. 1. The assumption of the simple harmonic form of the velocity potential along z-axis accounts for the oblique incident waves and maintains symmetry in the fluid motion. In the jth fluid region, the spatial velocity potential ϕ_j satisfies the partial differential equation

$$\frac{\partial^2\phi_j}{\partial x^2} + \frac{\partial^2\phi_j}{\partial y^2} - k_z^2\phi_j = 0, \tag{1}$$

along with the free-surface boundary condition given by

$$\frac{\partial\phi_j}{\partial y} + K\phi_j = 0 \quad \text{on} \quad y = 0, \tag{2}$$

where $K = \omega^2/g$ and g is the acceleration due to gravity. The bottom boundary condition is given by

$$\left.\begin{aligned} \tfrac{\partial\phi_j}{\partial y} = 0 \quad \text{on} \quad y = h \text{ (for finite water depth)},\\ \phi_j, \nabla\phi_j \to 0 \quad \text{as} \quad y \to \infty \text{ (for infinite water depth)}. \end{aligned}\right\} \tag{3}$$

On the vertical rigid wall, vanishing of horizontal velocity yields

$$\frac{\partial\phi_2}{\partial x} = 0, \quad \text{at} \quad x = L. \tag{4}$$

Assuming that the flexible plate is of uniform rigidity and is oscillating in the horizontal direction with displacement $\zeta(y,z,t) = Re\{\chi(y)e^{i(k_z z-\omega t)}\}$ where $\chi(y)$ is the complex deflection amplitude that is assumed to be the small compared to the water depth. The equation of motion for flexible plate acted upon by fluid pressure is given by (see [27,28])

$$EI\left(\frac{\mathrm{d}^2}{\mathrm{d}y^2} - k_z^2\right)^2\chi + Q\left(\frac{\mathrm{d}^2}{\mathrm{d}y^2} - k_z^2\right)\chi - m_s\omega^2\chi = i\rho\omega(\phi_1 - \phi_2), \quad \text{for} \quad x = 0, \quad y \in L_\mathrm{p}, \tag{5}$$

where EI is the uniform flexural rigidity of the plate, Q is the uniform compressive force acting on the plate, $m_s = \rho_s d$ is the uniform mass per unit length with ρ_s being material density of the elastic plate and d being the thickness of the plate that is assumed to be small, and ρ is the density of water. The boundary condition on the flexible porous plate is given by (see [7, p. 120])

$$\frac{\partial\phi_j}{\partial x} = ik_0G_0(\phi_1 - \phi_2) - i\omega\chi, \quad \text{for} \quad x = 0, \quad y \in L_\mathrm{p} \tag{6}$$

with G_0 being the porous-effect parameter as in Yu and Chwang [29]. Assuming that the plate is having free edge at $y = b$, vanishing of bending moment and shear force at the edge yields

$$\left(\frac{\mathrm{d}^2}{\mathrm{d}y^2} - \nu k_z^2\right)\chi = 0, \quad \left\{EI\left(\frac{\mathrm{d}^2}{\mathrm{d}y^2} - (2-\nu)k_z^2\right)\frac{\mathrm{d}}{\mathrm{d}y} + Q\frac{\mathrm{d}}{\mathrm{d}y}\right\}\chi = 0, \quad \text{at} \quad y = b, \tag{7}$$

where ν is the Poisson's ratio of the elastic plate. On the other hand, if the plate is having fixed edge at $y = a$, vanishing of the plate deflection and slope at the edge yields

$$\chi = 0, \quad \frac{\mathrm{d}\chi}{\mathrm{d}y} = 0 \quad \text{at} \quad y = a. \tag{8}$$

Moreover, the continuity of pressure and velocity in the gap yields

$$\left.\begin{aligned} \phi_1 &= \phi_2 \qquad \text{for } x = 0, \quad y \in L_{\mathrm{g}}, \\ \tfrac{\partial \phi_1}{\partial x} &= \tfrac{\partial \phi_2}{\partial x} \qquad \text{for } x = 0, \quad y \in L_{\mathrm{g}}. \end{aligned}\right\} \tag{9}$$

Finally, radiation condition is given by

$$\phi_1(x, y) \to \phi_0(x, y) + R\phi_0(-x, y) \quad \text{as} \quad x \to -\infty, \tag{10}$$

where R is the unknown amplitude of the reflected wave and $\phi_0(x, y)$ being the known incident wave potential. In the finite depth case, $\phi_0(x, y) = \{\cosh k_0(h - y)/\cosh k_0 h\}\mathrm{e}^{ik_x x}$ while $\phi_0(x, y) = \mathrm{e}^{ik_x x - Ky}$ in the infinite depth case, with $k_x = k_0 \cos\theta$ for finite water depth and $k_x = K\cos\theta$ for infinite water depth. Moreover, $k_z = k_0 \sin\theta$ for finite water depth and $K \sin\theta$ for infinite water depth with k_0 being the wave number associated with plane progressive wave in finite depth, satisfying dispersion relation $\omega^2 = gk_0 \tanh k_0 h$.

3. Formulation of system of integral equations

In this section, the boundary value problem, discussed in the aforementioned section, is converted into a system of integral equations following the procedure of Meylan [8]. Initially, using Green's function technique to the flexible plate equation and associated boundary conditions, an integral equation is derived. Then, applying Green's second identity to the velocity potential and the free-surface Green's function in the fluid domain, another system of three integral equations is derived. Further, using Green's second identity, explicit relation for the reflection coefficient is obtained in terms of the velocity potentials and their normal derivatives. Hereafter, the method of solution is described for a submerged plate as a general configuration with $L_{\mathrm{p}} = (a, b)$, and the problems of plate configurations such as surface-piercing and bottom-standing plates will be studied as particular cases in the numerical discussion.

It is observed that the boundary conditions in Eqs. (5), (7) and (8) is itself a Sturm–Liouville-type boundary value problem for $\chi(y)$. Thus, the associated Green's function $g_{\mathrm{p}}(\eta, y)$ satisfies

$$\frac{\mathrm{d}^4 g_{\mathrm{p}}}{\mathrm{d}\eta^4} + A\frac{\mathrm{d}^2 g_{\mathrm{p}}}{\mathrm{d}\eta^2} + Bg_{\mathrm{p}} = \delta(\eta - y), \quad \text{for} \quad a < y, \eta < b, \tag{11}$$

along with the boundary conditions (7) at $\eta = b$ and (8) at $\eta = a$. Further, the Green function $g_{\mathrm{p}}(\eta, y)$ satisfies the continuity and jump conditions given by

$$g_{\mathrm{p}}, \frac{\partial g_{\mathrm{p}}}{\partial \eta}, \frac{\partial^2 g_{\mathrm{p}}}{\partial \eta^2} \quad \text{are continuous at} \quad \eta = y, \tag{12}$$

and

$$\frac{\partial^3 g_{\mathrm{p}}}{\partial \eta^3}(y + 0, y) - \frac{\partial^3 g_{\mathrm{p}}}{\partial \eta^3}(y - 0, y) = -1. \tag{13}$$

The form of general solution $g_{\rm p}(\eta, y)$ is given by

$$g_{\rm p}(\eta,y)=\begin{cases} P_1\mathrm{e}^{\delta_1\eta}+Q_1\mathrm{e}^{-\delta_1\eta}+R_1\mathrm{e}^{\delta_2\eta}+S_1\mathrm{e}^{-\delta_2\eta}, & a<\eta<y<b\\ P_2\mathrm{e}^{\delta_1\eta}+Q_2\mathrm{e}^{-\delta_1\eta}+R_2\mathrm{e}^{\delta_2\eta}+S_2\mathrm{e}^{-\delta_2\eta}, & a<y<\eta<b. \end{cases}$$

where $\pm\delta_1$ and $\pm\delta_2$ are the distinct roots of the characteristic equation $q^4+Aq^2+B=0$ with $A=(Q/EI)-2k_z^2$, $B=k_z^4-(Q/EI)k_z^2-(m_s\omega^2/EI)$ being known parameters associated with the flexible plate equation given in Eq. (5). However, P_j, Q_j, R_j, S_j $(j=1,2)$ are unknown functions of y to be determined using the above-mentioned boundary conditions and the properties of Green's function (see [11]). Further, the expression for $g_{\rm p}(\eta, y)$ will be modified in an appropriate manner for $\delta_1=\delta_2$. Thus, using Green's function technique, the deflection $\chi(y)$ is obtained as

$$\chi(y)=\frac{i\rho\omega}{EI}\int\limits_{L_{\rm p}} g_{\rm p}(\eta,y)(\phi_1(\eta)-\phi_2(\eta))\,\mathrm{d}\eta,\quad y\in L_{\rm p}, \tag{14}$$

where $\phi_j(\eta)=\phi_j(0,\eta)$. Next, substituting $\chi(y)$ into (6) yields a Fredholm-type integral equation

$$\frac{\partial\phi_j}{\partial x}=ik_0G_0(\phi_1-\phi_2)+\frac{\rho\omega^2}{EI}\int\limits_{L_{\rm p}} g_{\rm p}(\eta,y)(\phi_1(\eta)-\phi_2(\eta))\,\mathrm{d}\eta,\ \text{ on }\ x=0,\ y\in L_{\rm p}. \tag{15}$$

Hereafter, the subscript j assigned to $\partial\phi/\partial x$ is removed since the normal velocity across the plate is continuous. Next, using the free-surface Green's function along with the continuity of velocity, three more Fredholm-type integral equations connecting ϕ_1, ϕ_2 and $\partial\phi/\partial x$ will be derived whose details are discussed separately for water of finite and infinite depths in the subsequent subsections.

3.1. Oblique wave trapping in finite water depth

Oblique wave trapping by a submerged vertical flexible porous plate involves the determination of the velocity potentials ϕ_1, ϕ_2 and the plate deflection χ along with the unknown constant R as discussed in Sect. 2. It may be noted that Eq. (15) is derived for the determination of ϕ_1, ϕ_2, and $\partial\phi/\partial x$. Thus, to derive a consistent system of Fredholm-type integral equations which relate these unknowns, application of Green's integral theorem to the functions $\phi_1(\xi,\eta)-(\cosh k_0(h-\eta)/\cosh k_0h)\mathrm{e}^{ik_x\xi}$ and $G(\xi,\eta;x,y)$ $(x<0)$ in a region of (ξ,η) plane bounded externally by the contour composed of the lines $\eta=0$, $-X\le\xi\le 0$; $\xi=-X$, $0\le\eta\le h$; $\eta=h$, $-X\le\xi\le 0$; $\xi=0$, $0\le\eta\le h$, and internally by a circle of very small radius ϵ with center at (x,y), which after taking the limits $X\to\infty$, $\epsilon\to 0$ and $x\to 0-$, yields

$$\phi_1(y)=2\phi_0(0,y)+\frac{1}{\pi}\int\limits_0^h\left\{\phi_1(\eta)\frac{\partial G(0,\eta;0,y)}{\partial n}-G(0,\eta;0,y)\frac{\partial\phi(\eta)}{\partial n}\right\}\mathrm{d}\eta,\quad \text{for } x=0-,\ y\in(0,h) \tag{16}$$

where $\partial/\partial n$ being the differentiation with respect to the outward drawn normal and $G(\xi,\eta;x,y)$ is the finite depth free-surface Green's function associated with oblique gravity wave problems (see [30]), given by

$$\begin{aligned} G(\xi,\eta;x,y)=&-4\pi ik_0\frac{\cosh k_0(h-\eta)\cosh k_0(h-y)}{k_x(2k_0h+\sinh 2k_0h)}\mathrm{e}^{ik_x|\xi-x|}\\ &-4\pi\sum_{n=1}^{\infty}\frac{k_n\cos k_n(h-\eta)\cos k_n(h-y)}{k_n'(2k_nh+\sin 2k_nh)}\mathrm{e}^{-k_n'|\xi-x|} \end{aligned}$$

with $k_n (n=1,2,3,\ldots)$ being the positive real roots of the dispersion relation $k\tan kh=-K$, $k_n'=(k_n^2+k_z^2)^{1/2}$. Hereafter, $\phi_j(0\mp,y)$ and $\partial\phi_j(0\mp,y)/\partial x$ are denoted as $\phi_j(y)$ and $\partial\phi(y)/\partial x$, respectively, as and when necessary.

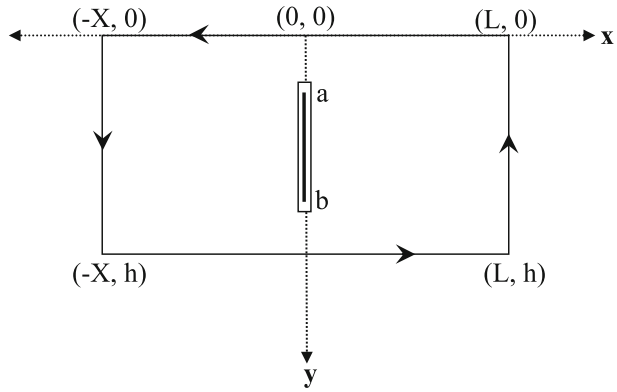

FIG. 2. Contour in the plane

Further, using the Green's second identity to the functions along the contours as discussed above and taking the limit $x \to -\infty$ instead of $x \to 0-$ and comparing the velocity potential with the far-field condition in Eq. (10), the reflected amplitude R is obtained as

$$R = \frac{2k_0 \cosh k_0 h}{k_x \left(2k_0 h + \sinh 2k_0 h\right)} \int_0^h \left[k_x \phi_1(\eta) - i \frac{\partial \phi(\eta)}{\partial n}\right] \cosh k_0 (h - \eta) \mathrm{d}\eta. \tag{17}$$

Similarly, applying Green's integral theorem to the functions $\phi_2(\xi, \eta)$ and $G(\xi, \eta; x, y)$ $(x > 0)$ in a region bounded externally by a contour, as in Fig. 2, that is composed of the lines $\eta = 0$, $0 \le \xi \le L$; $\xi = L$, $0 \le \eta \le h$; $\eta = h$, $0 \le \xi \le L$; $\xi = 0$, $0 \le \eta \le h$ and internally by a circle of very small radius ϵ with center at (x, y), and ultimately letting $\epsilon \to 0$ and $x \to 0+$, another Fredholm-type integral equation is derived as

$$\begin{aligned} \phi_2(y) = {} & \frac{1}{\pi} \int_0^h \left\{ \phi_2(\eta) \frac{\partial G(0, \eta; 0, y)}{\partial n} - G(0, \eta; 0, y) \frac{\partial \phi(\eta)}{\partial n} \right\} \mathrm{d}\eta \\ & - \frac{1}{\pi} \int_0^h \left\{ \phi_2(L, \eta) \frac{\partial G(L, \eta; 0, y)}{\partial n} \right\} \mathrm{d}\eta, \quad \text{for } x = 0+, \quad y \in (0, h). \end{aligned} \tag{18}$$

Proceeding in a similar manner as done for Eq. (18), taking the limit $x \to L-$ instead of $x \to 0+$, another Fredholm-type integral equation is derived as

$$\begin{aligned} \phi_2(y) = {} & \frac{1}{\pi} \int_0^h \left\{ \phi_2(\eta) \frac{\partial G(0, \eta; L-, y)}{\partial n} - G(0, \eta; L-, y) \frac{\partial \phi(\eta)}{\partial n} \right\} \mathrm{d}\eta \\ & - \frac{1}{\pi} \int_0^h \left\{ \phi_2(L, \eta) \frac{\partial G(L, \eta; L-, y)}{\partial n} \right\} \mathrm{d}\eta, \quad \text{for } x = L-, \quad y \in (0, h). \end{aligned} \tag{19}$$

Thus, Eqs. (15), (16), (18) and (19) yield a set of four coupled-integral equations for the determination of the unknown functions $\phi_1(0-, y)$, $\phi_2(0+, y)$, $\phi_2(L-, y)$ and $\partial\phi/\partial x$ in the finite depth case, and the scattering quantity R will be calculated using its explicit expression in Eq. (16).

3.2. Oblique wave trapping in infinite water depth

In this subsection, using similar contours as in case of finite depth with h being replaced by Y, and finally considering the limiting case $Y \to \infty$, three different integral equations are derived as

$$\phi_1(y) = \mathrm{e}^{-Ky} + \frac{1}{\pi}\int_0^\infty \left\{\phi_1(\eta)\frac{\partial G(0,\eta;0,y)}{\partial n} - G(0,\eta;0,y)\frac{\partial \phi(\eta)}{\partial n}\right\} \mathrm{d}\eta, \text{ for } x = 0-,\ y \in (0,\infty), \tag{20}$$

$$\begin{aligned}\phi_2(y) = {} & \frac{1}{\pi}\int_0^\infty \left\{\phi_2(\eta)\frac{\partial G(0,\eta;0+,y)}{\partial n} - G(0,\eta;0+,y)\frac{\partial \phi(\eta)}{\partial n}\right\}\mathrm{d}\eta \\ & -\frac{1}{\pi}\int_0^\infty \left\{\phi_2(L,\eta)\frac{\partial G(L,\eta;0+,y)}{\partial n}\right\} \mathrm{d}\eta, \text{ for } x = 0+,\ y \in (0,\infty)\end{aligned} \tag{21}$$

and

$$\begin{aligned}\phi_2(y) = {} & \frac{1}{\pi}\int_0^\infty \left\{\phi_2(\eta)\frac{\partial G(0,\eta;L-,y)}{\partial n} - G(0,\eta;L-,y)\frac{\partial \phi(\eta)}{\partial n}\right\}\mathrm{d}\eta \\ & -\frac{1}{\pi}\int_0^\infty \left\{\phi_2(L,\eta)\frac{\partial G(L,\eta;L-,y)}{\partial n}\right\} \mathrm{d}\eta, \text{ for } x = L-,\ y \in (0,\infty).\end{aligned} \tag{22}$$

where

$$\begin{aligned}G(\xi,\eta;x,y) = {} & K_0(k_z r) - K_0(k_z r') + \frac{2\pi i K}{(K^2 - k_z^2)^{1/2}}\ \mathrm{e}^{-K(y+\eta)+i(K^2-k_z^2)^{1/2}|x-\xi|} \\ & + 2\int_0^\infty \frac{k\{k\cos k(y+\eta) - K\sin k(y+\eta)\}}{(k^2+K^2)(k^2+k_z^2)^{1/2}}\ \mathrm{e}^{-(k^2+k_z^2)^{1/2}|x-\xi|}\ \mathrm{d}k,\end{aligned}$$

with $r = \{(x-\xi)^2 + (y-\eta)^2\}^{1/2}$, $r' = \{(x-\xi)^2 + (y+\eta)^2\}^{1/2}$ and $K_0(k_z r)$ is the zeroth- order modified Bessel function of the second kind. The derivation of G in the case of infinite water depth can be found in Levine [31]. In addition, the reflected amplitude is calculated as

$$R = \frac{K}{k_x}\int_0^\infty \left[k_x\phi_1(\eta) - i\frac{\partial \phi(\eta)}{\partial n}\right]\mathrm{e}^{-K\eta}\mathrm{d}\eta, \tag{23}$$

Thus, for the wave trapping in the case of infinite water depth, Eqs. (15) and (20)–(22) will be solved simultaneously and R can be computed subsequently.

3.3. Energy identity

In the study of surface wave scattering by floating/submerged structures, hydrodynamical relations such as energy identities are derived to understand the relationship between the scattered coefficients and to check the accuracy of the computational results. Often, the energy identities are derived using Green's integral theorem or law of conservation of energy flux. In case of water wave scattering by finite rigid plates, the energy identity is given by the relation $|R_0|^2 + |T_0|^2 = |A_0|^2$ where A_0, R_0 and T_0 are the incident, reflected and transmitted wave amplitudes, respectively. Unlike wave scattering by a barrier, in case of wave trapping by flexible porous plate near a wall, because of the fact that the region between the rigid wall and the flexible porous plate is finite, transmitted wave amplitude T will not appear in

the energy relation. In this subsection, using Green's second identity, energy relations for oblique wave trapping by a flexible porous plate located near a wall are derived in both the cases of water of finite and infinite depths separately.

Using Green's integral theorem to the function $\phi(x,y)$ and its complex conjugate $\bar{\phi}(x,y)$ in the region bounded by a contour as shown in Fig. 2, for finite water depth, it is derived that

$$\int_{\Gamma}\left(\phi\frac{\partial\bar{\phi}}{\partial n}-\bar{\phi}\frac{\partial\phi}{\partial n}\right)\mathrm{d}\Gamma=0,$$

where the contour Γ is composed of the lines $y=0$ $(-X\le x\le L)$; $x=L$ $(0\le y\le h)$; $y=h$ $(-X\le x\le L)$; $x=-X$ $(0\le y\le h)$ and $x=\pm 0(a\le y\le b)$. The contribution from the line $x=-X$ $(0\le y\le h)$ is obtained by taking the limit as $X\to\infty$, which yields

$$\frac{-ik_x(|R|^2-1)(2k_0h+\sinh 2k_0h)}{2k_0\cosh^2 k_0h}. \tag{24}$$

It can be easily checked that there is no contribution from the lines $y=0$ $(-X\le x\le L)$, $x=L$ $(0\le y\le h)$ and $y=h$ $(-X\le x\le L)$. Finally, the contribution from $x=\pm 0(a\le y\le b)$ is obtained as

$$\frac{\rho\omega^2}{EI}\int_a^b\int_a^b\left\{\bar{\mathcal{U}}(\eta,y)[\phi_1(y)-\phi_2(y)]-\mathcal{U}(\eta,y)\left[\bar{\phi}_1(y)-\bar{\phi}_2(y)\right]\right\}\mathrm{d}\eta\,\mathrm{d}y$$

$$-ik_0\int_a^b\left\{\bar{\mathcal{V}}(y)[\phi_1(y)-\phi_2(y)]+\mathcal{V}(y)[\bar{\phi}_1(y)-\bar{\phi}_2(y)]\right\}\mathrm{d}y, \tag{25}$$

where $\mathcal{U}(\eta,y)=g_{\mathrm{p}}(\eta,y)[\phi_1(\eta)-\phi_2(\eta)]$, $\mathcal{V}=G_0[\phi_1(\eta)-\phi_2(\eta)]$ and $\bar{\mathcal{U}}$, $\bar{\mathcal{V}}$, $\bar{\phi}_1$, $\bar{\phi}_2$ are the complex conjugates of the functions $\mathcal{U}$, $\mathcal{V}$, ϕ_1, ϕ_2, respectively. Thus, by summing up the results in (24) and (25), for finite depth case, we deduce an energy balance relation

$$|R|^2+|\gamma_1|+|\gamma_2|=1, \tag{26}$$

where

$$\gamma_1=\frac{i\rho\omega^2\mathcal{A}}{EI}\int_a^b\int_a^b\left\{\bar{\mathcal{U}}(\eta,y)\left[\phi_1(y)-\phi_2(y)\right]-\mathcal{U}(\eta,y)[\bar{\phi}_1(y)-\bar{\phi}_2(y)]\right\}\mathrm{d}\eta\,\mathrm{d}y\quad\text{and}$$

$$\gamma_2=k_0\mathcal{A}\int_a^b\left\{\bar{\mathcal{V}}(y)[\phi_1(y)-\phi_2(y)]+\mathcal{V}(y)[\bar{\phi}_1(y)-\bar{\phi}_2(y)]\right\}\mathrm{d}y,$$

with

$$\mathcal{A}=-\frac{2k_0\cosh^2 k_0h}{k_x(2k_0h+\sinh 2k_0h)}. \tag{27}$$

Proceeding in a similar manner, it is easy to check that in case of infinite water depth, the energy identity satisfies the relation in (26) with k_0 being K and $\mathcal{A}$ being replaced by $-K/k_x$.

4. Numerical results and discussions

As discussed in the aforementioned section, the study of oblique wave trapping by flexible porous plates leads to a system of four integral equations involving $\phi_1(0-,y)$, $\phi_2(0+,y)$, $\phi_2(L-,y)$ and $\partial\phi/\partial n$ in finite/semi-infinite intervals. To evaluate various integrals associated with the above-mentioned integral equations, Gauss–Legendre quadrature formula is used for evaluating integrals over finite intervals while,

for integrals in semi-infinite intervals, Gauss–Laguerre quadrature formula is used with the assumption that the velocity potentials and their normal derivatives decrease exponentially. The two Gauss quadrature formulae are briefly discussed for clarity (as in [33]).

The Gauss–Legendre quadrature formula is given by

$$\int_a^b f(x)\mathrm{d}x \approx \frac{b-a}{2}\sum_{j=1}^{n} w_j f\left(\frac{b-a}{2}x_j + \frac{b+a}{2}\right) \tag{28}$$

where $x_j (j = 1, 2, \ldots, n)$ are the zeros of Legendre polynomial $P_n(x)$ of degree n, and the weight functions $w_j (j = 1, 2, \ldots, n)$ are given by

$$w_j = \frac{2}{\left(1 - x_j\right)^2 \left(P_n'(x_j)\right)^2} \tag{29}$$

with $P_n^{'}(x)$ being the derivative of $P_n(x)$. On the other hand, for function $f(x)$ which decays exponentially in the interval $(0, \infty)$, the Gauss–Laguerre quadrature formula is given by

$$\int_0^\infty f(x)\mathrm{d}x \approx \sum_{j=1}^{n} w_j f(x_j) \tag{30}$$

where x_js are the zeros of the Laguerre polynomial $L_n(x)$ of degree n, and corresponding weight functions w_js are given by

$$w_j = \frac{(j!)^2}{L_n^{'}(x_j) L_{n+1}(x_j)}, \tag{31}$$

with $L_n^{'}(x)$ being the derivative of $L_n(x)$.

In order to solve the system of integral equations derived for finite and infinite water depths, the above-mentioned quadrature formulae will be used depending upon the nature of the integral. Hereafter, oblique wave trapping by flexible porous plates of three different configurations discussed in the previous sections will be analyzed separately. For the numerical computation, values of various physical parameters are kept fixed as $G_0 = 0.5 + 0.5i$, $m_1 = m_s/(\rho c) = 0.01$, $\nu = 0.3$, $\gamma = EI/(\rho g c^4) = 0.1$, $\beta = Q/(\rho g c^2) = 0.05$, and $\theta = 30^\circ$ unless it is mentioned. Further, in the non-dimensionalization of the flexural rigidity EI and mass m_s, c refers to b in case of infinite water depth, and c refers to either b or h depending on the nature of the physical boundary and plate configurations which will be highlighted as and when required for water of finite depth. In the present study, it is found that the characteristic equation associated with the plate equation in Sect. 3 has distinct roots. For the wave trapping problems, the reflection coefficients are computed using the formulae

$$K_r = |R|. \tag{32}$$

Equation (26) yields the energy relation in the form given by

$$\mathcal{E} = 1, \tag{33}$$

with $\mathcal{E} = K_\mathrm{r}^2 + |\gamma_1| + |\gamma_2|$. The non-dimensional horizontal wave forces on the flexible porous plate K_f and the vertical rigid wall K_w are given by the formulae

$$K_\mathrm{f} = \frac{\omega}{gc^2}\left|\int_{L_\mathrm{p}} (\phi_1(0, y) - \phi_2(0, y))\mathrm{d}y\right|, \tag{34}$$

and

$$K_\mathrm{w} = \frac{\omega}{gc^2}\left|\int_{L_\mathrm{w}} (\phi_2(L, y))\mathrm{d}y\right|, \tag{35}$$

TABLE 1. *Energy identity for bottom-standing plate in water of finite depth with* $k_0h = 1$, $a/h = 0.4$, $\gamma = 0.1$, $\beta = 0.05$, $G_0 = 0.5 + 0.5i$ *and* $\theta = 30^\circ$

L/λ	K_r	$\lvert\gamma_1\rvert$	$\lvert\gamma_2\rvert$	$\mathcal{E}$
1.0	0.8400	0.0005	0.2943	1.0004
1.5	0.7346	0.0009	0.4502	0.9907
2.0	0.6551	0.0014	0.5608	0.9913
2.5	0.6629	0.0012	0.5704	1.0110
3.0	0.8207	0.0007	0.3164	0.9906

TABLE 2. *Energy identity for surface-piercing plate in water of finite depth with* $k_0h = 1$, $b/h = 0.6$, $\gamma = 0.1$, $\beta = 0.05$, $G_0 = 0.5 + 0.5i$ *and* $\theta = 30^\circ$

L/λ	K_r	$\lvert\gamma_1\rvert$	$\lvert\gamma_2\rvert$	$\mathcal{E}$
1.0	0.7677	0.0011	0.4005	0.9909
1.5	0.6259	0.0020	0.6081	1.0018
2.0	0.4891	0.0025	0.7507	0.9924
2.5	0.4197	0.0032	0.8237	1.0030
3.0	0.6389	0.0016	0.5817	0.9914

, respectively, with c being the same as defined above and L_w span over the water depth. Further, the non-dimensional form of the structural displacements $\varsigma(y)$ is given by

$$\varsigma(y) = \frac{\rho\omega}{EI\,h}\Big|\int_{L_\mathrm{p}} g(\eta, y)[\phi_1(0,\eta) - \phi_2(0,\eta)]\mathrm{d}\eta\Big|. \tag{36}$$

In order to check the accuracy of the computational results, the numerical results are validated by comparing the results obtained in the present paper with known results in the literature and the energy identity derived in the previous section. Moreover, computational results for the surface-piercing and submerged plates are obtained based on the assumption that the upper end of the plate near the free surface is fixed and the submerged end is free. On the other hand, for the bottom-standing plate, numerical results are obtained assuming that the submerged end is free and the edge near the bottom bed is fixed.

Tables 1 and 2 show the values of the reflection coefficient K_r, wave energy transformation due to the plate deformation γ_1 and wave energy dissipation by the porous plate γ_2 for various values of normalized distance between the porous plate and the rigid wall L/λ for bottom-standing and surface-piercing flexible porous plates, respectively. It is clear from both Tables 1 and 2 that energy loss due to porosity is higher compared to that of plate deformation. Further, Tables 1 and 2 depict that for a particular value of L/λ, wave reflection is higher for bottom-standing plate compared to that of surface-piercing plate, and reverse trend is observed for energy loss due to dissipation by the porous plate. This may be because of the fact that wave energy concentration is more near the free surface, which is dissipated more by the surface-piercing plate compared to the bottom-standing plate. From both the tables, it is concluded that the computational results for the reflection coefficient satisfy the energy identity for bottom-standing and surface-piercing plates in water of finite depth which demonstrates the accuracy of the computational results.

4.1. Bottom-standing flexible porous plate

In this subsection, various numerical results on oblique wave trapping by the bottom-standing flexible porous plate are studied in finite water depth while the corresponding results in infinite water depth are not considered as mentioned in Sect. 2. The accuracy and convergence of the numerical results are

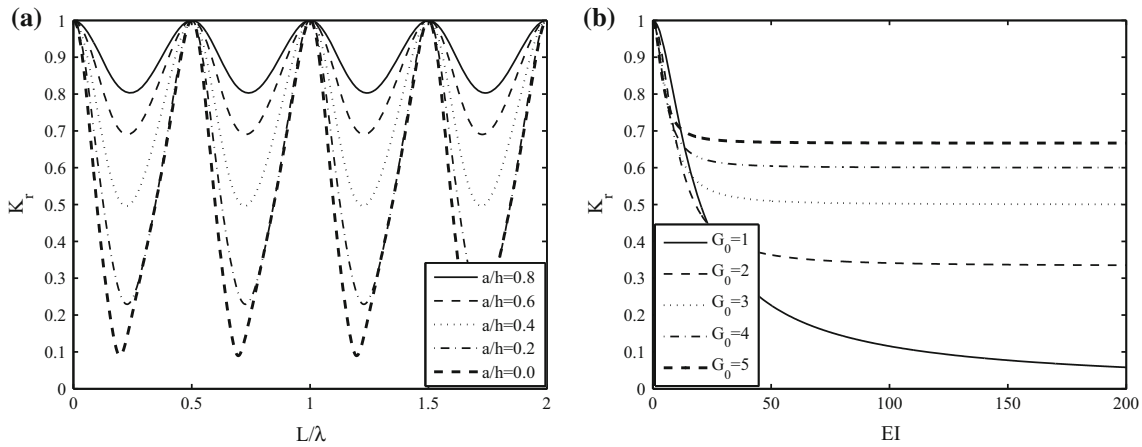

FIG. 3. Variation of the reflection coefficient versus **a** L/λ for different values of a/h with $\gamma = 0.1$, $G_0 = 1.0$ and **b** structural rigidity EI (MN-m) for different values of G_0 with $a/h = 0.0$, $\beta = 0.0$, $k_0 h = 1.0$, $\theta = 0^\circ$ and $L/\lambda = 0.25$

verified by comparing the reflection coefficients for wave trapping by a flexible porous plate as in Fig. 3a, b with known results in the literature followed by discussion on various physical parameters related to wave trapping in the subsequent figures.

In Fig. 3a, the reflection coefficient K_r versus normalized distance between the plate and the rigid wall L/λ is plotted for different values of gap length a/h. Here, the computational results for K_r agree well with the results of figure 2 in Yip et al. [23]. It is observed that the reflection coefficient changes periodically as L/λ increases. As the distance between the plate and the rigid wall L becomes an integer multiple of half of the wavelength of the incident waves, full-wave reflection occurs irrespective of the gap length a/h. Further, Fig. 3a depicts that between two consecutive maxima in wave reflection, minima in the wave reflection takes place. The minima in wave reflection is referred as partial wave trapping as in Yip et al. [23]. Next, the reflection coefficient K_r versus structural rigidity EI is plotted in Fig. 3b for different values of porous-effect parameter G_0. The reflection coefficient plotted in Fig. 3b agrees well with Fig. 2d of Wang and Ren [22]. Figure 3b depicts that with an increase in the structural rigidity, reflection coefficient decreases until it reaches a uniform pattern. Further, it can be observed that for highly flexible plate, structural porosity has negligible effect on wave reflection which may be due to the predominant role of higher modes of vibration of the highly flexible plate.

In Fig. 4a, b, the reflection coefficient K_r versus normalized distance between the flexible porous plate and the rigid wall L/λ and angle of incidence θ are plotted, respectively, for different values of the porous-effect parameter G_0. From both the figures, it is observed that with the increase in the absolute value of the porous-effect parameter G_0, reflection coefficient increases. This may be because of the fact that with the increase in plate porosity, more wave energy passes through the porous plate which in turn is reflected by the rigid wall. Figure 4a shows that irrespective of the values of the porous-effect parameter G_0, full reflection occurs for the same values of L/λ. However, a comparison with Fig. 3a reveals that for nonzero angle of incidence θ, full reflection does not occur at $L/\lambda = n/2$ with n being a positive integer. Further, Fig. 4a depicts that as the absolute value of the porous-effect parameter G_0 increases, the minima in the wave reflection shifted to the right. This may be due to the phase change of the reflected waves as the absolute value of the porous-effect parameter G_0 increases. On the other hand, Fig. 4b depicts that with an increase in angle of incidence θ, wave reflection increases in an oscillatory pattern. This pattern in wave reflection with the variation in angle of incidence is completely different from the oblique wave scattering by flexible porous plate of similar configurations as observed in Koley et al. [11].

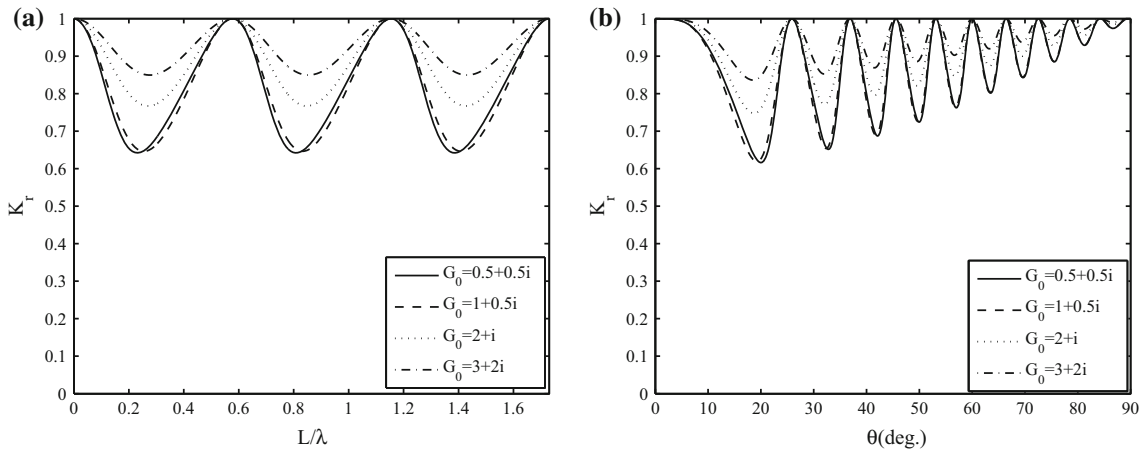

FIG. 4. Variation of the reflection coefficient K_r versus **a** L/λ with $\theta = 30^\circ$ and **b** angle of incidence θ for different values of G_0 with $a/h = 0.4$, $k_0h = 1.0$, $L/\lambda = 5$ and $\gamma = 0.1$

Figure 5a shows the variation of reflection K_r versus k_0h for different values of the gap length a/h. It is observed that near $k_0h = 0$, i.e., in case of long waves, zero reflection occurs for complete plate while full reflection occurs for the same k_0h for partial plates irrespective of plate length. However, in the case of partial plate, due to presence of gap, wave diffraction occurs (as in [32]), which tends to transmit all the waves for smaller values of k_0h which is reflected back by the rigid wall. A reverse pattern was observed in case of wave scattering by a bottom-standing flexible plate as in Koley et al. [11]. On the other hand, for moderate values of k_0h, i.e., for intermediate water depth, minimum reflection occurs in case of partial plate which is because of the destructive interference between the incident and reflected waves whereas maximum reflection occurs in case of a complete plate which is due to the constructive interference between the incident and reflected waves. Further, in case of deep water, with an increase in wave number k_0h, wave reflection increases for bottom-standing partial plates of any length while wave reflection decreases for complete plate. Moreover, Fig. 5a depicts that for partial plates, as the plate length increases, wave reflection decreases. In Fig. 5b, the reflection coefficient K_r versus non-dimensional structural rigidity γ is plotted for different values of porous-effect parameter G_0. Figure 5b reveals that as the absolute value of the porous-effect parameter G_0 increases, wave reflection increases. Further, it is observed that for values of structural rigidity γ close to zero, regardless of the variation in the porous-effect parameter G_0, almost full reflection occurs which may be due to the predominate role of higher modes of vibration of the flexible structure. However, wave reflection attends certain minimum for moderate value of structural rigidity γ, which increases and attends an uniform steady state with further increase in structural rigidity γ. The minimum in wave reflection for moderate values of structural rigidity may be due to the mutual interaction of different structural modes of vibration with the incident and reflected waves. Further, for higher values of structural rigidity, the flexible structure behaves like a rigid body and thus wave reflection follows a steady pattern.

Figure 6a shows the displacement profiles of the bottom-standing plate for various values of the structural rigidity γ. It is observed that with an increase in structural rigidity γ, plate deflection decreases. This may be due to the reason that as the structural rigidity increases, flexible plate tends to behave like a rigid plate. Further, plate deflection is zero near the bottom bed as the plate is fixed near the bottom and maximum deflection takes place at the submerged free edge for moderate values of structural rigidity. Moreover, for highly flexible plate, the plate deflection is very high because of the predominant role of higher modes of vibration of the plate under wave action. On the other hand, in Fig. 6b, the free-surface elevation $\bar{\eta}/h$ versus x/h is plotted for different values of gap length a/h. It is observed that

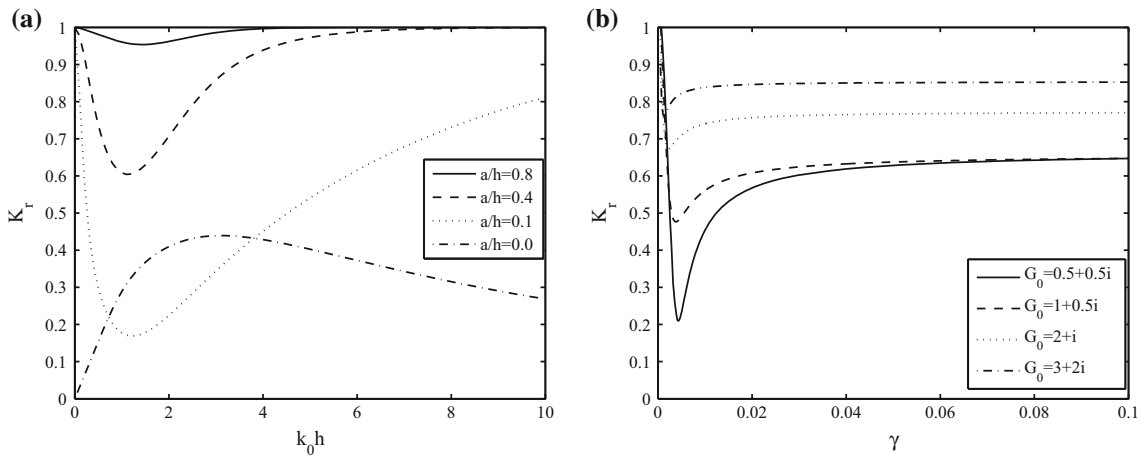

FIG. 5. Variation of the reflection coefficient versus **a** k_0h for different values of a/h with $G_0 = 1.0$, $\theta = 0^\circ$ and **b** structural rigidity γ for different values of G_0 with $a/h = 0.4$, $\beta = 0.0$, $k_0h = 1.0$, $\theta = 30^\circ$ and $L/\lambda = 0.25$

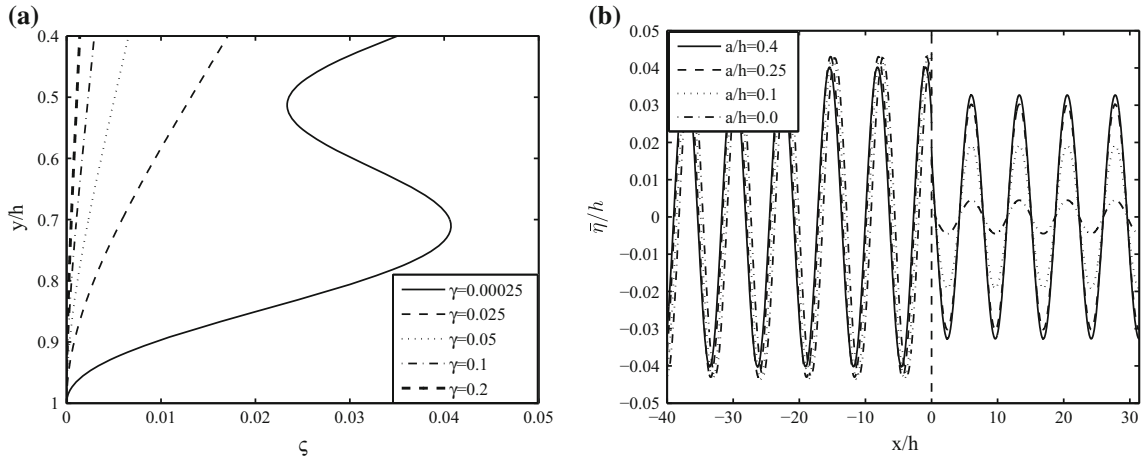

FIG. 6. Displacement profiles for various values structural rigidity γ with $a/h = 0.4$ and **b** free-surface elevation for various values of gap length a/h with $\gamma = 0.1$, $G_0 = 0.5 + 0.5i$, $\beta = 0.05$, $k_0h = 1.0$, $\theta = 30^\circ$ and $L/\lambda = 5$

the free-surface elevation in the confined region decreases with a decrease in the gap length a/h. This may be because of the fact that with a decrease in the gap length, more wave energy gets trapped in the confined region between the porous plate and the rigid wall as observed in Fig. 3a.

Figure 7a, b depicts the instantaneous velocity field in Regions 1 and 2 as in Fig. 1 at $t = 0$. In Fig. 7a, the horizontal scale has taken same as the vertical scale, while in Fig. 7b, the distance between the plate and the rigid wall has taken same as wavelength of the incident wave. Figure 7a illustrates that the flow velocity is higher near the free surface. This may be due to the fact that in case of bottom-standing plate, the fluid can pass freely in the gap region above the plate. On the other hand, Fig. 7b reveals that the flow velocity near the free surface adjacent to the rigid wall is predominant in the vertically downward direction which is negligible at the sea bed. Further, along the interface of the porous plate, the flow direction is neither horizontal nor vertical which is because of the energy dissipation by the

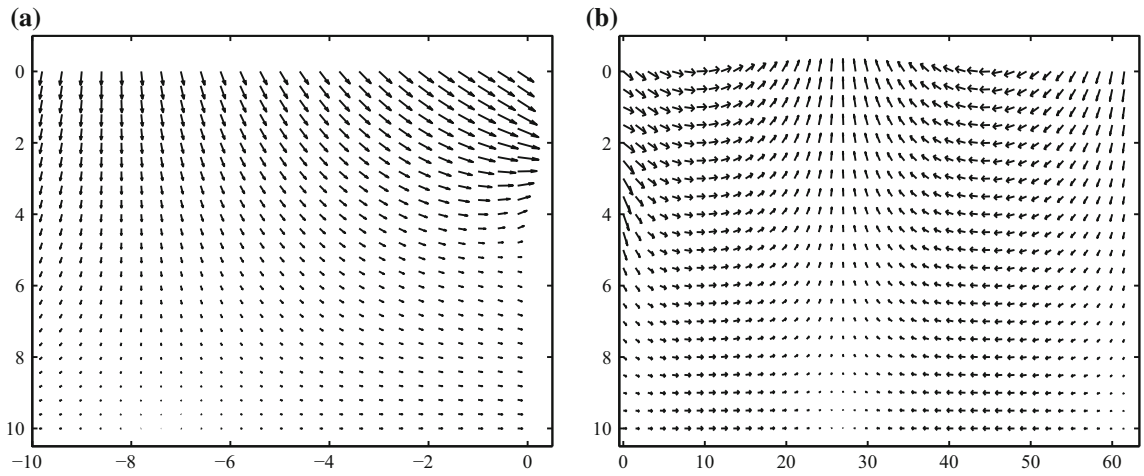

FIG. 7. Flow field for **a** left-hand region of the plate and **b** confined region between the plate and the rigid wall for $a/h = 0.4$, $G_0 = 0.5 + 0.5i$, $\beta = 0.05$, $\gamma = 0.1$, $k_0 h = 1.0$, $\theta = 30^\circ$ and $L/\lambda = 1.0$

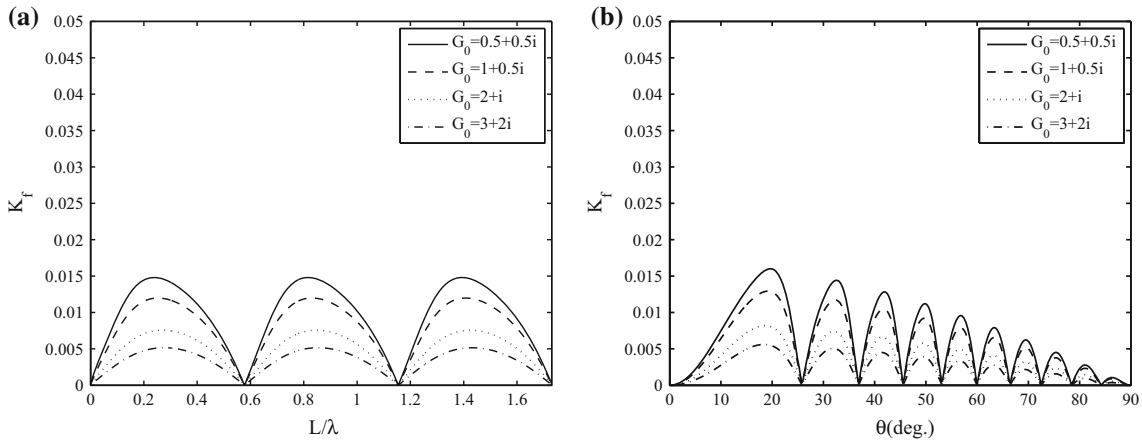

FIG. 8. Variation of the wave force K_f versus **a** L/λ with $\theta = 30^\circ$ and **b** angle of incidence θ for different values of G_0 with $a/h = 0.4$, $k_0 h = 1.0$, $L/\lambda = 5$ and $\gamma = 0.1$

flexible porous plate. However, at the interface region along the gap, the flow velocity is comparatively higher than that along the porous plate. Further, near the bottom bed along the porous plate, the flow velocity in the vertical direction is negligible. Moreover, in the confined zone near $L = \lambda/2$, seiches are formed where flow direction remains in the vertically upward direction.

Figure 8a, b shows the variations of the wave forces exerted on the plate K_f versus the normalized distance between the plate and the rigid wall L/λ and the angle of incidence θ for various values of porous-effect parameter G_0, respectively. Both the figures reveal that as the absolute value of the porous-effect parameter G_0 increases, wave force exerted on the plate decreases. This may be due to the fact that with an increase in the absolute value of the porous-effect parameter G_0, more wave energy passes through the fine pores of the plate and thus less force is exerted on the plate. A comparison with Fig. 4 shows the values of L/λ and θ for which full reflection occurs, and no wave force is exerted on the plate. Moreover, the values of L/λ and θ for which minimum wave reflection occurs correspond to the situation

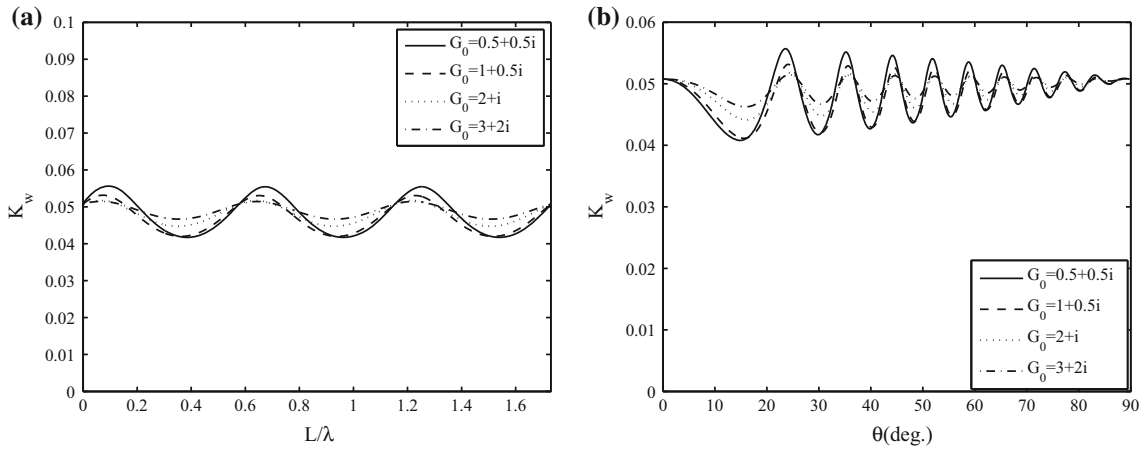

FIG. 9. Variation of the wave force K_w versus **a** L/λ with $\theta = 30^\circ$ and **b** angle of incidence θ for different values of G_0 with $a/h = 0.4$, $k_0h = 1.0$, $L/\lambda = 5$ and $\gamma = 0.1$

of maximum force on the plate which ensures that during trapping, wave force exerted on the plate becomes maximum.

Figure 9a, b shows the variations of the wave forces exerted on the rigid wall K_w versus the normalized distance between the plate and the rigid wall L/λ and the angle of incidence θ for various values of porous-effect parameter G_0, respectively. From both the figures, it is observed that optima in wave load is observed for moderate values of the porous-effect parameter $G_0 = 0.5 + 0.5\,\mathrm{i}$. Further, a comparison with Fig. 8 reveals the values of L/λ and angle of incidence θ ($0^\circ < \theta < 90^\circ$) for which wave force exerted on the plate becomes maximum, and wave force exerted on the rigid wall becomes minimum. However, for angle of incidence θ close to 0° and 90°, forces acting on the porous plate become zero and on the rigid wall remain the same.

4.2. Surface-piercing flexible porous plate

In this subsection, various numerical results on oblique wave trapping by the surface-piercing flexible porous plate are studied in both the cases of finite and infinite water depths. Although major results are discussed for finite depth, results on finite and infinite water depths are compared in various cases.

In Fig. 10a, b, the reflection coefficient K_r versus normalized distance between the flexible porous plate and the rigid wall L/λ and angle of incidence θ are plotted, respectively, for different values of porous-effect parameter G_0. It is observed that with an increase in the absolute value of the porous-effect parameter G_0, reflection coefficient increases. The overall pattern of Fig. 10 is same as that of bottom-standing plate as in Fig. 4. However, a comparison of Fig. 10 with Fig. 4 reveals that wave reflection is higher in case of bottom-standing plate compared to the surface-piercing plate. This may be due to the reason that wave energy concentration is more near the free surface, which is dissipated more by the surface-piercing plate compared to the bottom-standing plate. Thus, less wave energy is reflected back by the rigid wall for a surface-piercing plate. Therefore, it can be concluded that a surface-piercing plate is more suitable for developing an effective wave trapping system.

Figure 11a shows the variation of the reflection coefficient K_r versus k_0h for different values of the plate length b/h. It is observed that for fully extended plate, reflection coefficient becomes zero near $k_0h = 0$, whereas for the same values of k_0h, full reflection occurs for partial plate. The observation is similar to that in case of bottom-standing plate. However, more energy is reflected back in case of bottom-standing plate compared to the surface-piercing plate of similar configurations. Thus, a bottom-standing plate is

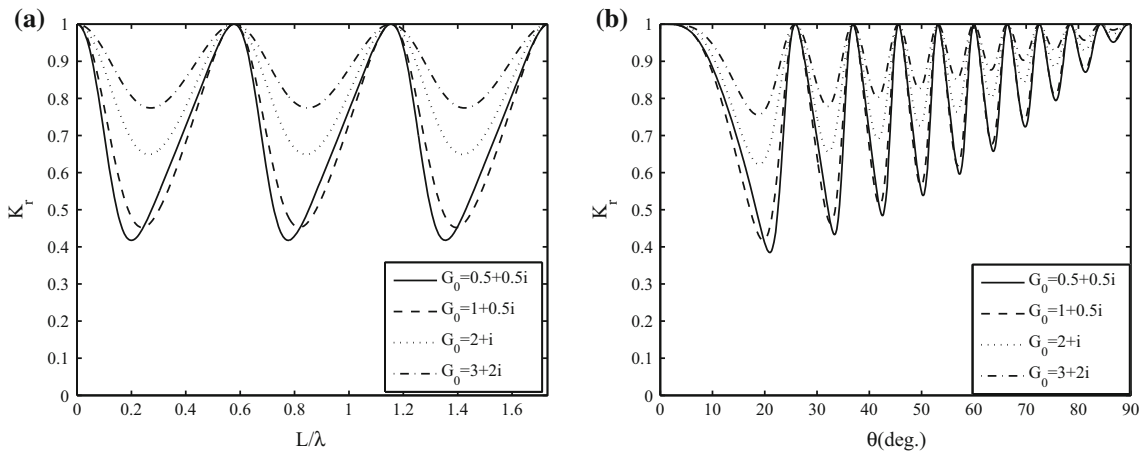

FIG. 10. Variation of the reflection coefficient K_r versus **a** L/λ with $\theta = 30^\circ$ and **b** angle of incidence θ for different values of G_0 with $b/h = 0.6$, $k_0 h = 1.0$, $L/\lambda = 5$ and $\gamma = 0.1$

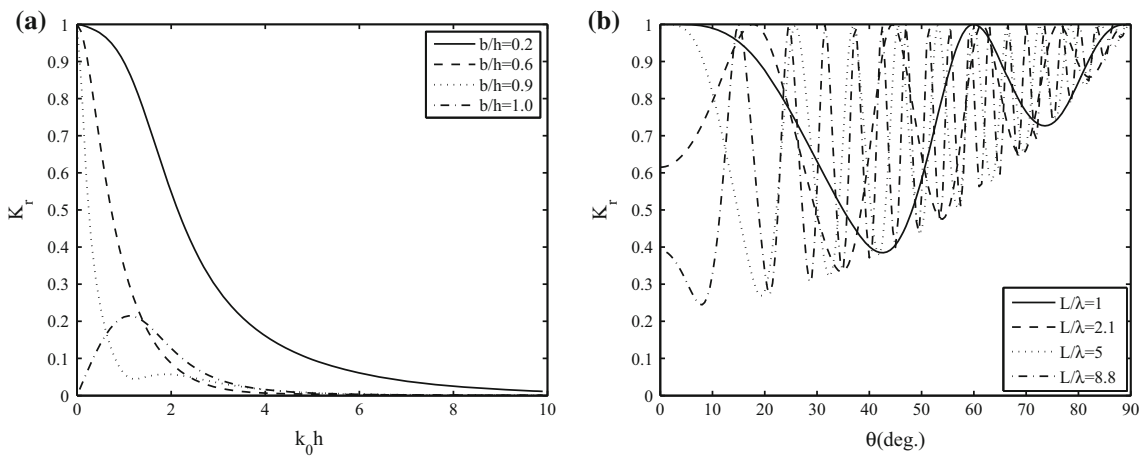

FIG. 11. Variation of the reflection coefficient versus **a** $k_0 h$ for different values of b/h with $\theta = 0^\circ$ and **b** angle of incidence θ for different values of L/λ with $b/h = 0.6$, $\gamma = 0.1$, $k_0 h = 1.0$ and $G_0 = 1.0$

preferred for maximum wave reflection. On the other hand, in Fig. 11b, reflection coefficient K_r versus angle of incidence θ is plotted for various values of L/λ. It is observed that the minima in the wave reflection increases with an increase in the angle of incidence. Further, it can be seen that number of full reflection increases as L/λ increases, while the global minimum in the reflection coefficient decreases as L/λ increases. The occurrences of the minima in the wave reflection for certain angle of incidence may be due to the destructive interference between the incident and the reflected waves.

Figure 12a shows the displacement profiles of the surface-piercing plate for various values of the structural rigidity γ. It is observed that with an increase in structural rigidity γ, plate deflection decreases. Further, Fig. 12a depicts that the plate with moderate structural rigidity γ, deflection is more near the submerged end having free edges. Moreover, plate deflection is zero near the free surface as the plate is fixed near the free surface. A comparison with Fig. 6a shows that the plate deflection is more in case of surface-piercing plate compared to the bottom-standing plate of the same configurations. On the other

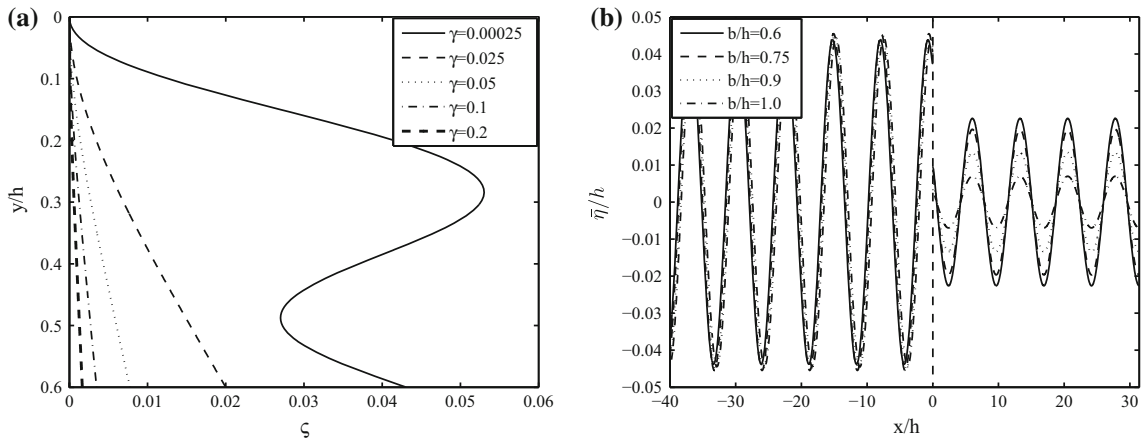

FIG. 12. Displacement profiles for various values structural rigidity γ with $b/h = 0.6$ and **b** free-surface elevation for various values of plate length b/h with $\gamma = 0.1$, $G_0 = 0.5 + 0.5i$, $\beta = 0.05$, $k_0 h = 1.0$, $\theta = 30^\circ$ and $L/\lambda = 5$

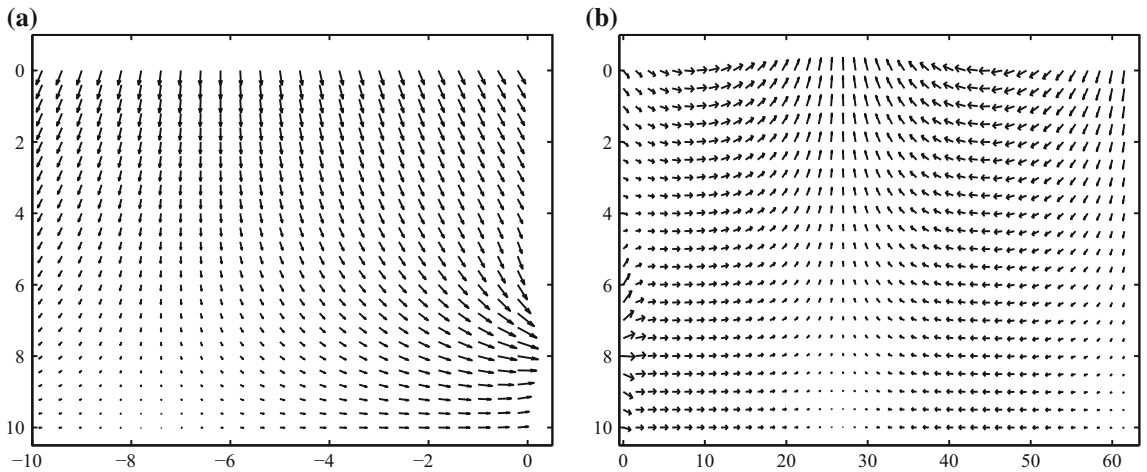

FIG. 13. Flow field for **a** left-hand region of the plate and **b** confined region between the plate and the rigid wall for $b/h = 0.6$, $G_0 = 0.5 + 0.5i$, $\beta = 0.05$, $\gamma = 0.1$, $k_0 h = 1.0$, $\theta = 30^\circ$ and $L/\lambda = 1.0$

hand, Fig. 12b shows that the free-surface elevation $\bar{\eta}/h$ versus x/h for different values of plate length b/h. It is observed that the free-surface elevation in the confined region decreases as the plate length b/h increases. A comparison with Fig. 6b reveals that in the confined zone, free-surface elevation is less in case of surface-piercing plate as compared with the bottom-standing plate. This may be due to the fact that a surface-piercing plate dissipates more wave energy concentrating near the free surface.

Figure 13a, b depicts the instantaneous velocity field at $t = 0$ in Regions 1 and 2 as in Fig. 1. In Fig. 13a, the horizontal scale remains the same as the vertical scale, while in Fig. 13b, the distance between the plate and the rigid wall remains the same as the wavelength of the incident wave. Figure 13a depicts that near the plate, the flow velocity is higher in the gap region compared to the free surface as the plate obstructs the wave motion and a major amount of wave energy passes through the gap below the plate. However, in the region far from the plate, the flow velocity is higher near the free surface compared to the bottom as the concentration of the wave energy is higher near the free surface than the bottom.

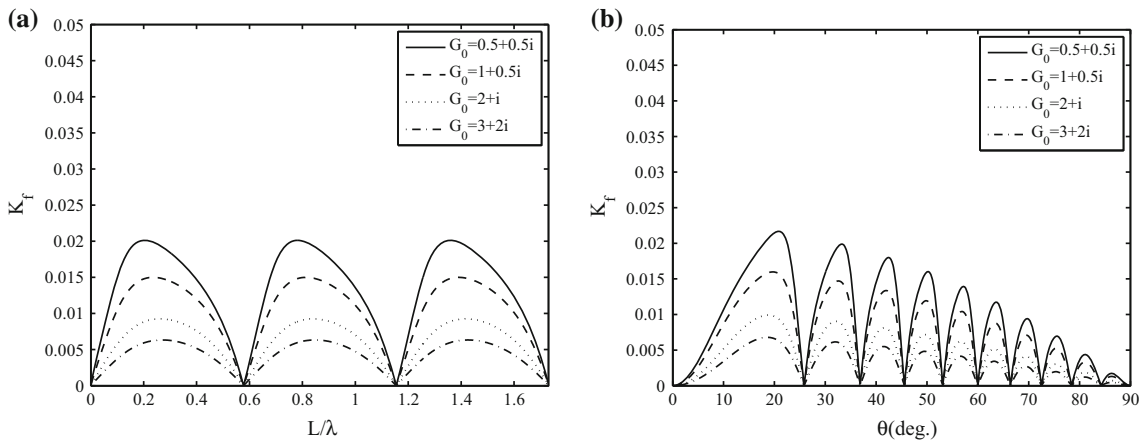

FIG. 14. Variation of the wave force K_f versus **a** L/λ with $\theta = 30^\circ$ and **b** angle of incidence θ for different values of G_0 with $b/h = 0.6$, $k_0h = 1.0$, $L/\lambda = 5$ and $\gamma = 0.1$

On the other hand, Fig. 13b reveals that due to the energy dissipation by the porous plate, the flow direction is neither vertical nor horizontal along the interface of the plate. Moreover, the flow velocity is comparatively higher through the gap than through the porous plate. Further, a comparison with Fig. 7b shows that in both the cases of bottom-standing and surface-piercing plate, seiches are formed in the tranquility zone near $L = \lambda/2$, where flow direction remains vertically upward. This is because of the mutual interaction of the wave motion within the confined zone between the surface-piercing plate and the rigid wall. Moreover, near the rigid wall, horizontal velocity is zero and wave energy excitation is in the vertically downward direction which is negligible near the bottom bed.

Figure 14a, b shows the variations of the wave forces exerted on the plate K_f versus the normalized distance between the plate and the rigid wall L/λ and the angle of incidence θ for various values of porous-effect parameter G_0, respectively. Form both the figures, it is observed that with an increase in the absolute value of the porous-effect parameter G_0, wave force exerted on the plate decreases. Further, the value of L/λ for which trapping occurs as in Fig. 10, wave force on the plate becomes maximum while the situation of full reflection corresponds to zero wave force on the plate. This observation is similar to that of the bottom-standing plate as in Fig. 8. However, a comparison with Fig. 8 reveals that wave force exerted on the surface-piercing plate is higher than that of the bottom-standing plate.

Figure 15a, b depicts the variations of the wave forces exerted on the rigid wall K_w versus the normalized distance between the plate and the rigid wall L/λ and the angle of incidence θ for various values of porous-effect parameter G_0, respectively. From both the figures, it is observed that wave force exerted on the rigid wall K_w increases with an increase in the absolute value of the porous-effect parameter G_0 and angle of incidence θ except for certain values of L/λ and θ for which maxima in the wave reflection occurs. Further, a comparison with Fig. 14 reveals that maxima in the wave force exerted on the rigid wall K_w corresponds to the minima in the wave force exerted on the plate K_f. Similar phenomena is observed in case of bottom-standing plate as in Fig. 9. Further, a comparison with Fig. 9 shows that although in both the cases, the reflection coefficient is oscillatory in nature but the amplitude of oscillation is higher in case of surface-piercing plate compared to that of the bottom-standing plate.

In Fig. 16a, b, the reflection coefficient K_r versus the normalized distance between the plate and the rigid wall L/b and the angle of incidence θ are plotted for different values of water depth k_0h. Both the figures illustrate that minimum in wave reflection decreases with an increase in water depth. This is because of the fact that as water depth increases, wave energy concentration near the free surface increases and is dissipated by the surface-piercing plate. Further, from Fig. 16a, it is observed that as

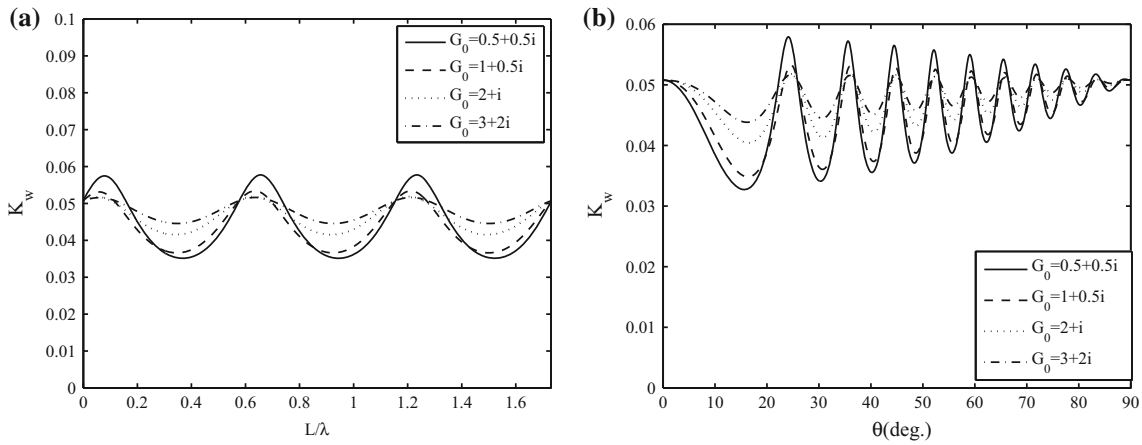

FIG. 15. Variation of the wave force K_{w} versus **a** L/λ with $\theta = 30^{\circ}$ and **b** angle of incidence θ for different values of G_0 with $b/h = 0.6$, $k_0 h = 1.0$, $L/\lambda = 5$ and $\gamma = 0.1$

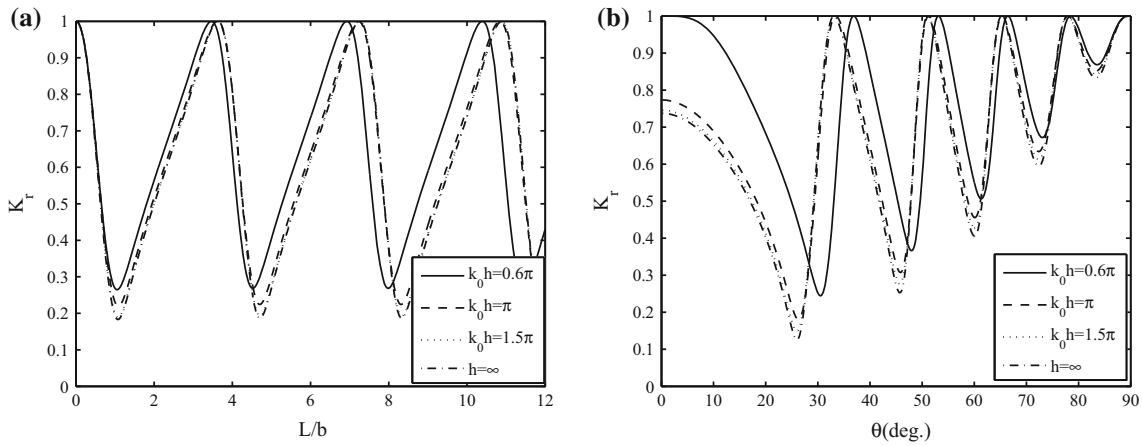

FIG. 16. Variation of the reflection coefficient versus **a** L/b with $\theta = 30^{\circ}$ and **b** angle of incidence θ for different values of $k_0 h$ with $\gamma = 0.1$, $G_0 = 0.5 + 0.5i$, $\beta = 0.05$ and $L/b = 15$

water depth increases, the optima in the reflection coefficient occurs for different values of the distance between the plate and the rigid wall L/b. This may be due to the change in wave characteristics such as wave length and amplitude with the change in water depth. On the other hand, Fig. 16b depicts that near $\theta = 0^{\circ}$, as water depth increases, wave reflection decreases. However, as the angle of incidence θ increases, the reflection coefficient K_{r} increases in an oscillatory pattern and finally converges at $\theta = 90^{\circ}$ irrespective of water depth.

In Fig. 17a, b, reflection coefficient K_{r} and wave force exerted on the plate K_{f} versus structural rigidity γ are plotted for different values of water depth, respectively. Figure 17a reveals that with an increase in water depth, reflection coefficient increases. Further, it is observed that initially, the reflection coefficient K_{r} decreases to attend certain minimum which increases and becomes uniform for higher values of structural rigidity γ. For very small values of γ close to zero, full reflection occurs which is independent of water depth. For smaller values of structural rigidity γ, due to the destructive interference of higher

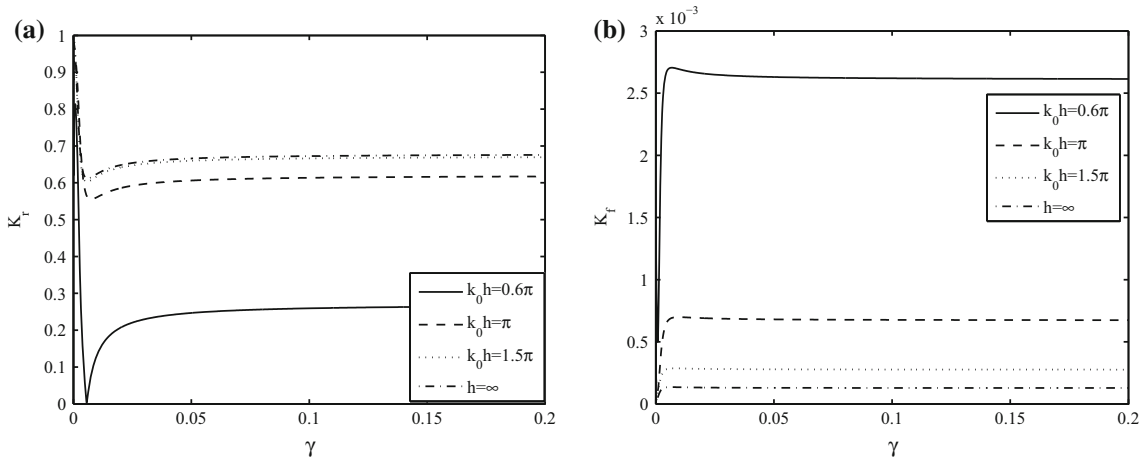

FIG. 17. Variation of the **a** reflection coefficient K_r and **b** wave force K_f versus structural rigidity γ for different values of k_0h with $G_0 = 0.5 + 0.5i$, $\beta = 0.0$, $\theta = 30°$ and $L/b = 15$

modes of vibration of the flexible plate with the incident waves, wave reflection attends certain minimum. However, for larger values of structural rigidity γ, the flexible plate tends to behave like a rigid plate and thus wave reflection is least affected with change in structural rigidity γ. On the other hand, Fig. 17b shows that as the non-dimensional water depth k_0h increases, wave force exerted on the plate decreases. Further, a comparison with Fig. 17a shows that maxima in wave reflection corresponds to the minima in the wave force.

4.3. Submerged flexible porous plate

In Fig. 18a, b, reflection coefficient K_r versus normalized distance between the plate and rigid wall L/λ and angle of incidence θ are plotted for various values of the porous-effect parameter G_0, respectively. From both the figures, it is observed that wave reflection increases with an increase in the absolute value of the porous-effect parameter G_0 which is similar to the observations made in case of surface-piercing and bottom-standing plates. A comparison with Figs. 4 and 10 reveals that wave reflection is more for a submerged plate compared to a surface-piercing plate and less compared to a bottom-standing plate. Further, a comparison with Figs. 4 and 10 demonstrates that irrespective of plate configurations, full reflection occurs for the same distance between the plate and the rigid wall L/λ and for the same angle of incidence θ.

In Fig. 19a, b, the instantaneous velocity field is plotted at $t = 0$ for Regions 1 and 2 as in Fig. 1. In Fig. 19a, the horizontal scale remains the same as the vertical scale, while in Fig. 19b, the distance between the plate and the rigid wall remains the same as the wavelength of the incident wave. Figure 19a depicts that the flow velocity adjacent to the submerged plate is higher in the horizontal direction near the free surface and near to the bottom bed compared to the plate region. On the other hand, Fig. 19b depicts that in the confined zone between the submerged plate and the rigid wall, the direction of flow is similar to that of the bottom-standing and surface-piercing plates. However, the flow speed remains almost uniform within the confined zone which may be due to the uniform distribution of the wave energy in the confined zone. Moreover, a comparison with Figs. 7 and 13 shows that in all the cases, seiches are formed near $L/\lambda = 0.5$. However, near $L/\lambda = 0.5$, the vertical motion is very small in the case of submerged plate compared to the bottom-standing and surface-piercing plates.

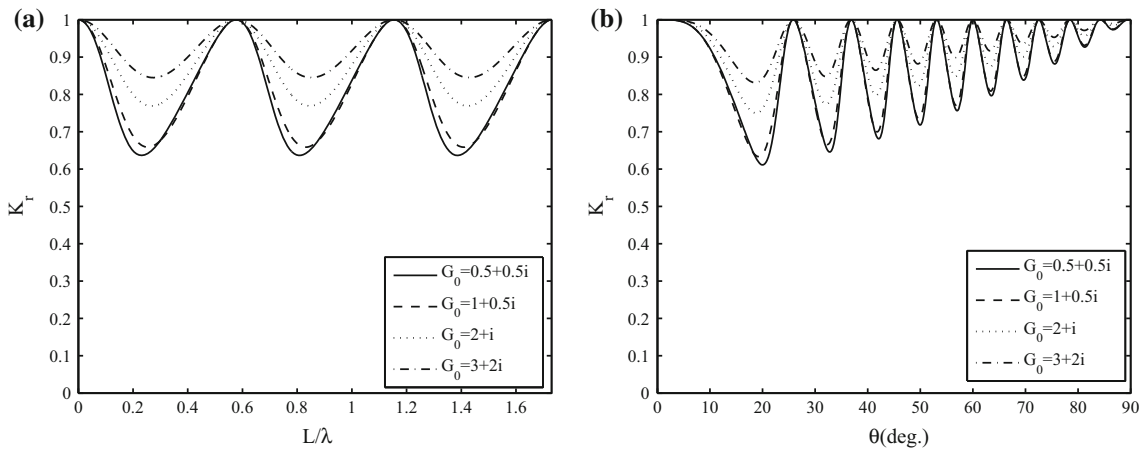

FIG. 18. Variation of the reflection coefficient K_r versus **a** L/λ with $\theta = 30^\circ$ and **b** angle of incidence θ for different values of G_0 with $a/h = 0.2$, $b/h = 0.8$, $k_0h = 1.0$, $L/\lambda = 5$ and $\gamma = 0.1$

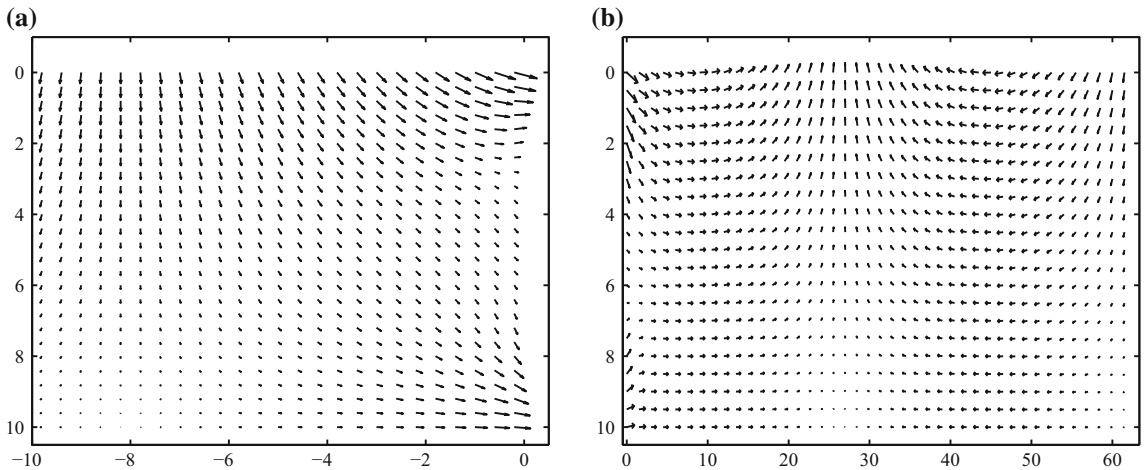

FIG. 19. Flow field for **a** left-hand region of the plate and **b** confined region between the plate and the rigid wall for $a/h = 0.2$, $b/h = 0.8$, $G_0 = 0.5 + 0.5i$, $\beta = 0.05$, $\gamma = 0.1$, $k_0h = 1.0$, $\theta = 30^\circ$ and $L/\lambda = 1.0$

Figure 20a, b shows the variation of the wave force exerted on the plate K_f versus the normalized distance between the plate and the rigid wall L/λ and the angle of incidence θ for various values of the porous-effect parameter G_0, respectively. Both the figures reveal that wave force acting on the plate K_f decreases as the absolute value of the porous-effect parameter G_0 increases. A comparison with Figs. 8 and 14 demonstrate that wave force K_f exerted on the plate is less in case of submerged plate compared to the bottom-standing and surface-piercing plate, which may be due to the uniform distribution of the wave energy in the confined region as discussed in Fig. 19. Moreover, it can be seen that irrespective of the plate configurations, wave force K_f vanishes for the same distance between the plate and the rigid wall L/λ and the angle of incidence θ.

In Fig. 21a, b, wave force exerted on the rigid wall K_w versus normalized distance between the plate and the rigid wall L/λ and angle of incidence θ are plotted for various values of the porous-effect parameter G_0, respectively. Both the figures illustrate that wave force acting on the rigid wall K_w increases as the

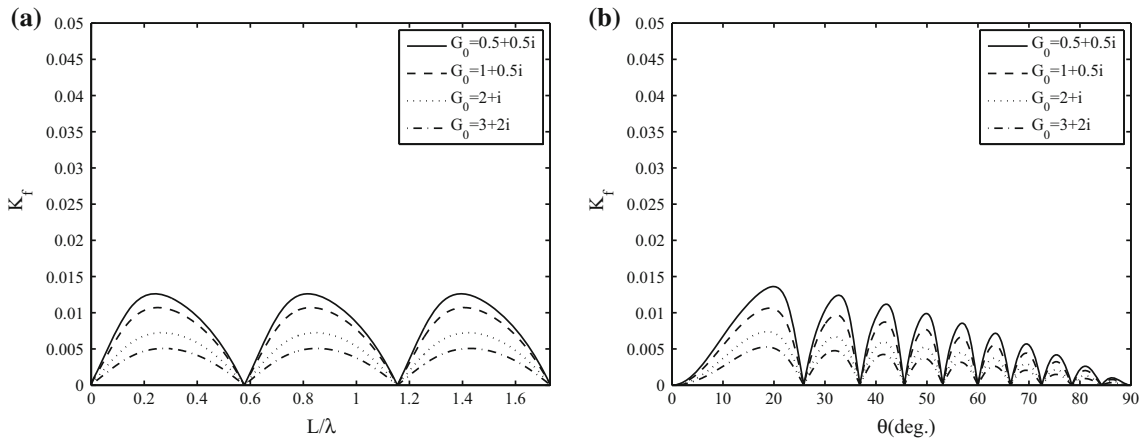

FIG. 20. Variation of the wave force K_f versus **a** L/λ with $\theta = 30^\circ$ and **b** angle of incidence θ for different values of G_0 with $a/h = 0.2$, $b/h = 0.8$, $k_0h = 1.0$, $L/\lambda = 5$ and $\gamma = 0.1$

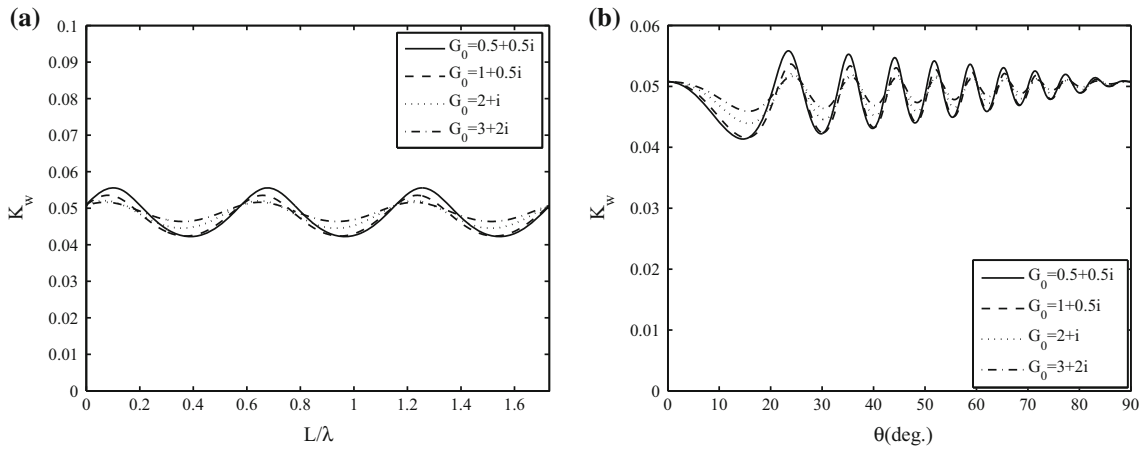

FIG. 21. Variation of the wave force K_w versus **a** L/λ with $\theta = 30^\circ$ and **b** angle of incidence θ for different values of G_0 with $a/h = 0.2$, $b/h = 0.8$, $k_0h = 1.0$, $L/\lambda = 5$ and $\gamma = 0.1$

absolute value of the porous-effect parameter G_0 increases. Further, wave force exerted on the rigid wall is more for the submerged plate compared to the surface-piercing plate and is similar to that of the bottom-standing plate as in Figs. 9 and 15, respectively. Further, a comparison with Figs. 9 and 15 shows that irrespective of the plate configurations, wave force acted on the rigid wall K_w becomes minimum for the same distance between the plate and the rigid wall L/λ and for the same angle of incidence θ.

Figure 22a, b depicts the reflection coefficient K_r versus the normalized distance between the plate and the rigid wall $L/(b-a)$ and the angle of incidence θ for different values of water depth k_0h, respectively. In both the figures, it is observed that as water depth increases, the wave reflection decreases. Further, Fig. 22a shows that with an increase in water depth, the optima in the reflection coefficient changes and occurs for different values of the distance between the plate and the rigid wall $L/(b-a)$. This may be due to the fact that as water depth increases, the wavelength increases and thus less wave energy is reflected back by the rigid wall. On the other hand, in Fig. 22b, it is observed that near $\theta = 0^\circ$, wave reflection decreases as the water depth increases. However, as the angle of incidence θ increases and approaches to 90°, the reflection coefficients K_r increase in an oscillatory pattern and finally converges at $\theta = 90^\circ$ for

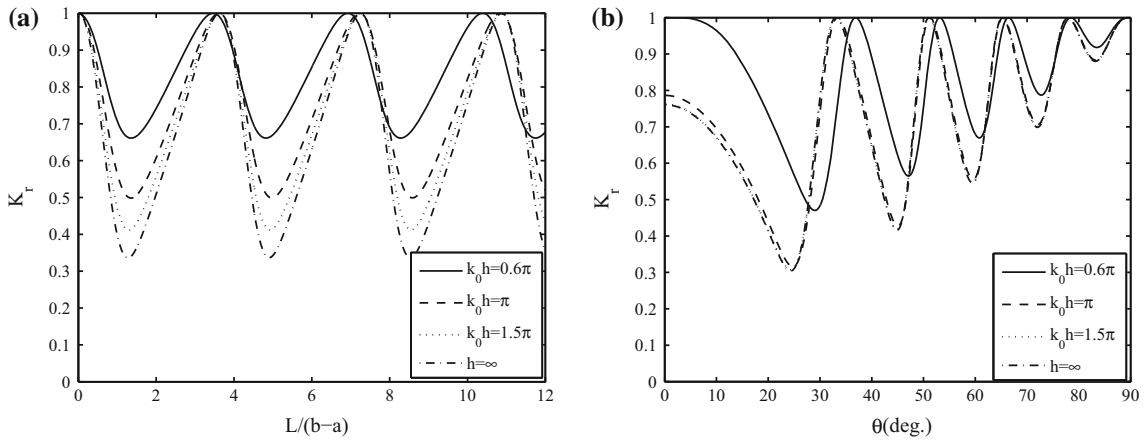

FIG. 22. Variation of the reflection coefficient versus **a** $L/(b-a)$ with $\theta = 30^\circ$ and **b** angle of incidence θ for different values of k_0h with $\gamma = 0.1$, $G_0 = 0.5 + 0.5i$, $\beta = 0.05$ and $L/(b-a) = 15$

different water depth. A comparison with Fig. 16 illustrates that wave reflection is less in case of surface-piercing plate compared to that of submerged plate in finite as well as infinite water depth. Further, Figs. 16, 17 and 22 reveal that wave reflection in infinite water depth is close to the finite depth results for higher values of k_0h which means that wave reflection in case of infinite water depth is comparable to that in case of deep water waves.

5. Conclusions

The present study deals with trapping of oblique water waves by a submerged flexible porous plate located at a finite distance from a rigid wall in water of finite and infinite depths. Results for bottom-standing and surface-piercing flexible porous plates are derived and analyzed as special cases from the general formulation of the submerged plate. Using Green's function technique, a system of four integral equations is derived which are handled for solution using appropriate Gauss quadrature formulae. Accuracy of the computational results is demonstrated by substituting the computed values of the reflection coefficients in the derived energy identity for the bottom-standing and surface-piercing plates in water of finite depth. It is observed that the flexibility of a plate is not much effective without porosity. However, with moderate porosity, a flexible plate can act as an effective barrier for dissipating unwanted wave energy. For developing an effective wave trapping system, the effectiveness of the surface-piercing plate over the bottom-standing as well as submerged plate is analyzed by comparing various numerical results. Further, certain comparisons among reflection coefficients and wave forces acting on the plate and the rigid wall have been demonstrated, and it is observed that for suitable combination of porous-effect parameter and, distance between the plate and the rigid wall, full reflection is associated with zero force on the flexible porous plate. Moreover, maximum wave load on the flexible porous plate is associated with minimum wave load on the rigid wall and vice versa irrespective of plate configurations. A comparison of the flow velocity within the confined zone demonstrates that for oblique wave trapping by submerged flexible porous plate, flow speed within the confined zone is more uniform compared to the bottom-standing and surface-piercing plates. However, flow direction within the confined zone remains similar regardless of the plate configuration. A comparison of results on finite and infinite water depths reveals that results for higher values of the non-dimensional water depth k_0h are similar to results in infinite water depth. Irrespective of plate configuration, it is found that for very long waves, negligible wave reflection occurs when the plate is complete while, due to wave diffraction through the gap, full reflection occurs for

partial flexible porous plates irrespective of plate length. From the present study, it can be concluded that using flexible porous plates of suitable configuration located at a finite distance from a rigid wall, wave load on the rigid wall can be reduced to a minimum and suitable tranquility zone can be created for protecting existing marine structures. The present study is likely to play a significant role in the protection of existing vertical walls from wave impact by introducing a flexible porous plate near coastal infrastructure. The same concept can also be used in the design of new rigid walls in marine environment which can withstand the wave load to a great extent.

Acknowledgments

S.K. acknowledges the financial support received as a senior research fellow from Council of Scientific and Industrial Research, New Delhi, to pursue this research work.

References

1. Zhu, S., Chwang, A.T.: Experimental studies on caisson-type porous seawalls. Exp. Fluids **33**, 512–515 (2002)
2. Williams, A.N., Wang, K.H.: Flexible porous wave barrier for enhanced wetlands habitat restoration. J. Eng. Mech. **129**, 1–8 (2003)
3. Dean, W.R.: On the reflection of surface waves by submerged plane barrier. Proc. Camb. Philos. Soc. **44**, 483–491 (1945)
4. Ursell, F.: The effect of a fixed vertical barrier on surface waves in deep water. Proc. Camb. Philos. Soc. **43**, 374–382 (1947)
5. Mandal, B.N., Chakrabarti, A.: Water Wave Scattering by Barriers. WIT Press, Southampton (2000)
6. Linton, C.M., McIver, P.: Handbook of Mathematical Techniques for Wave/Structure Interactions. Chapman and Hall/CRC, New York (2001)
7. Sahoo, T.: Mathematical Techniques for Wave Interaction with Flexible Structures. Chapman and Hall/CRC Press, London (2012)
8. Meylan, M.H.: A flexible vertical sheet in waves. Int. J. Offshore Polar Eng. **5**(2), 105–110 (1995)
9. Chakraborty, R., Mandal, B.N.: Water wave scattering by an elastic thin vertical plate submerged in finite depth water. J. Mar. Sci. Appl. **12**, 393–399 (2013)
10. Chakraborty, R., Mandal, B.N.: Scattering of water waves by a submerged thin vertical elastic plate. Arch. Appl. Mech. **84**, 207–217 (2014)
11. Koley, S., Kaligatla, R.B., Sahoo, T.: Oblique wave scattering by a vertical flexible porous plate. Stud. Appl. Math. 1–34 (2015). doi:10.1111/sapm.12076
12. Stokes, G.G.: Report on recent researches in hydrodynamics. Report to 16th Meeting of the British Association for the Advancement of Science, Southampton, Murrey, London 1–20 (1846)
13. Ursell, F.: Trapping modes in the theory of surface waves. Proc. Camb. Philos. Soc. **47**, 347–358 (1951)
14. Jones, D.S.: The eigen values of $\nabla^2 u - \lambda u = 0$ when the boundary conditions are given on semi-infinite domains. Proc. Camb. Philos. Soc. **49**, 668–684 (1953)
15. Greenspan, H.P.: A note on edge waves in a stratified fluid. Stud. Appl. Math. **49**(4), 381–388 (1970)
16. Leblond, P.H., Mysak, L.A.: Waves in the Ocean. Elsevier, Amsterdam (1978)
17. Linton, C.M., Evans, D.V.: Trapped modes above a submerged horizontal plate. Q. J. Mech. Appl. Math. **44**(3), 487–506 (1991)
18. Linton, C.M., McIver, M.: The interaction of waves with horizontal cylinders in two-layer fluids. J. Fluid. Mech. **304**, 213–229 (1995)
19. Kuznetsov, N., Maz'ya, V., Vainberg, V.: Linear Water Waves: A Mathematical Approach. Cambridge University Press, UK (2004)
20. Sahoo, T., Lee, M.M., Chwang, A.T.: Trapping and generation of waves by vertical porous structures. J. Eng. Mech. **126**, 1074–1082 (2000)
21. Chwang, A.T., Dong, Z.: Wave-trapping due to a porous plate. In: Proceedings of the 15th Symposium on Naval Hydrodynamics, pp. 407–417. National Academy Press, Washington, DC (1984)
22. Wang, K.H., Ren, X.: An effective wave-trapping system. Ocean Eng. **21**(2), 155–178 (1994)
23. Yip, T.L., Sahoo, T., Chwang, A.T.: Trapping of waves by porous and flexible structures. Wave Motion **35**, 41–54 (2002)
24. Behera, H., Mandal, S., Sahoo, T.: Oblique wave trapping by porous and flexible structures in a two-layer fluid. Phys. Fluids **25**, 1–23 (2013)

25. Koley, S., Behera, H., Sahoo, T.: Oblique wave trapping by porous structures near a wall. J. Eng. Mech. ASCE **141**(3), 1–15 (2015)
26. Behera, H., Sahoo, T.: Gravity wave interaction with porous structures in two-layer fluid. J. Eng. Math. **87**, 73–97 (2014)
27. Clough, R.B., Penzien, J.: Dynamics of Structures. McGraw-Hill, New York (1975)
28. Williams, A.N., Geiger, P.T., McDogal, W.G.: Flexible floating breakwater. J. Waterw. Port Coast. Ocean Eng. ASCE **117**(5), 429–450 (1991)
29. Yu, X., Chwang, A.T.: Wave induced oscillation in harbor with porous breakwaters. J. Waterw. Port Coast. Ocean Eng. ASCE **120**(2), 125–144 (1994)
30. Rhee, J.P.: A note on the diffraction of obliquely incident water waves by a stepwise obstacle. Appl. Ocean Res. **23**, 299–304 (2001)
31. Levine, H.: Scattering of surface waves by a submerged circular cylinder. J. Math. Phys. **6**, 1231–1234 (1965)
32. Tuck, E.O.: Transmission of water waves through small apertures. J. Fluid Mech. **49**, 65–74 (1971)
33. Ralston, A.: A First Course in Numerical Analysis. McGraw Hill, New York (1965)

R. B. Kaligatla, S. Koley and T. Sahoo
Department of Ocean Engineering and Naval Architecture
Indian Institute of Technology Kharagpur
Kharagpur,
721302 West Bengal
India
e-mail: tsahoo@naval.iitkgp.ernet.in;
tsahoo1967@gmail.com

Present Address:
R. B. Kaligatla
Department of Applied Mathematics
Indian School of Mines
Dhanbad
India

(Received: September 18, 2014)